Synthesis, optical and electrochemical properties of a series of push-pull dyes based on the 4,4-bis(4-methoxy phenyl)butadienyl donor

Corentin Pigot, Guillaume Noirbent, Thanh-Tuân Bui, Sébastien Péralta, Sylvain Duval, Malek Nechab, Didier Gigmes, Frédéric Dumur

Synthesis, optical and electrochemical properties of a series of push-pull dyes based on the 4,4-*bis*(4-methoxy phenyl)butadienyl donor

Corentin Pigot [1], Guillaume Noirbent [1], Thanh-Tuân Bui [2], Sébastien Péralta [2], Sylvain Duval [3], Malek Nechab [1], Didier Gigmes [1] and Frédéric Dumur [1,*]

[1] Aix Marseille Univ, CNRS, ICR UMR7273, F-13397 Marseille France
[2] CY Cergy Paris Université, LPPI, F-95000 Cergy, France
[3] Université de Lille, CNRS, Centrale Lille, ENSCL, Univ. Artois, UMR 8181 - UCCS - Unité de Catalyse et Chimie du Solide, F-59000 Lille, France

* Correspondence: frederic.dumur@univ-amu.fr

Abstract

A series of twelve dyes based on the 4,4-*bis*(4-methoxyphenyl)butadienyl donor and differing by the electron acceptors have been designed and synthesized. The different dyes were characterized by UV-visible absorption spectroscopy as well as cyclic voltammetry. By fine tuning the electron-accepting ability of the fourteen selected acceptors, dyes absorbing between 400 and 650 nm could be obtained with this π-extended donor. To get a deeper insight into the optical properties, solvatochromism was investigated in 23 different solvents and remarkable linear correlations could be obtained using the Taft and Catalan solvatochromism scales. A comparison with four dyes used as reference compounds and differing from the series of twelve dyes by the structure of the electron-donating groups was also established so that the electron releasing ability of the 4,4-*bis*(4-methoxyphenyl)butadienyl donor could be compared with the reference ones. To prepare these four references compounds, only two electron acceptors previously used for the design of the twelve dyes have been employed. Interestingly, variation of the absorption maxima of the twelve dyes was determined as being more influenced by the polarizability of the solvent rather than by its polarity. To support the experimental results, theoretical calculations were carried out.

Keywords:

Push-pull dyes, Michler's aldehyde, solvatochromism, TNF, TCF, rhodanine, indanedione

1. Introduction

During the past decades, organic dyes have been the subject of numerous research efforts due to the wide range of applications in which these dyes are involved, ranging from emitters for organic light-emitting diodes,[1-3] chromophores for organic solar cells,[4-6] dyes for Non-Linear Optical applications,[7-9] fluorescent probes for various biological applications,[10-11] photoinitiators of polymerization,[12-21] sunlight induced polymerization [22-26] or photoredox catalysis.[27-30] When dyes of high molar extinction coefficients are researched, an effective strategy to get this intense absorption consists in developing molecules in which the electron donor is separated from the electron acceptor by mean of a conjugated spacer.[31-32] As a result of the presence of both an electron donating and an electron-accepting group, a strong electronic delocalization within the π-conjugated system can occur, giving rise in the visible range to an intense absorption band corresponding to the intramolecular charge transfer (ICT) band. To enhance the molar extinction coefficient, the oscillation strength should be increased, what can be obtained by increasing the number of electrons involved in the electronic delocalization. In this aim, elongation of the π-conjugated spacer is an effective strategy which was applied to the design of numerous dyes.[33-35] Parallel to this, the π-conjugated spacer being included into the Highest Occupied Molecular Orbitals (HOMO), a destabilization of the HOMO level is jointly observed, reducing the HOMO-LUMO gap (where LUMO stands for Lowest Unoccupied Molecular Orbital) and red-shifting the absorption. Among electron donors, the 4,4-*bis*(aryl)butadienyl donors have been identified as promising candidates for the design of dyes exhibiting a pronounced solvatochromism.[36-37] Besides, the number of push-pull dyes designed with these electron-releasing groups remain scarce, as exemplified by the dyes **PP1-PP35** reported in the Figure 1.[38-42] If most of these structures have been examined for their solvatochromic properties, it has to be noticed that **PP6**, **PP28**, **PP29**, **PP31**, **PP33**, **PP34** and **PP35** have been tested as photoinitiators of polymerization due to their strong absorption extending over the visible range.[41] Conversely, **PP30** and **PP32** have been specifically designed as proligands to complex metal cations[40] whereas **PP19** and **PP20** have only been reported as structures. To date, the 4,4-*bis*(4-methoxyphenyl)butadienyl donor has only been scarcely used for the design of push-pull dyes since only three dyes i.e. **PP5**, **PP11** and **PP17** are reported to date. Besides, numerous electron acceptors are reported in the literature[43] so that this electron donor deserves to be studied with a wider range of electron acceptors. As earlier mentioned, push-pull dyes are now extensively studied as photoinitiators of polymerization activable in the visible range and under low light intensity.

Fine tuning of the absorption properties over the visible range is therefore an urgent need of photopolymerists. Indeed, an optimal monomer conversion can be achieved while adjusting the absorption maxima of dyes with the emission wavelengths of the light sources. Therefore, all electron donors, even if weak electron donors, can be of interest to design dyes whose absorption maxima could coincide with the emissions of the irradiation sources. Parallel to this, the substitution pattern of dyes can drastically impact the solubility of dyes in resins. Therefore, investigations of new groups that can improve the solubility of dyes in resins is also a key parameter governing the polymerization efficiency.

In this work, a series of twelve dyes **PP5**, **PP6**, **PP11**, **PP15** and **D1-D9** differing by the electron acceptors have been designed and synthesized (See Figure 2). The different dyes have been characterized by different techniques including UV-visible absorption spectroscopy and cyclic voltammetry. Parallel to this, the solvatochromic properties of the different dyes have been examined while using different solvatochromic scales.

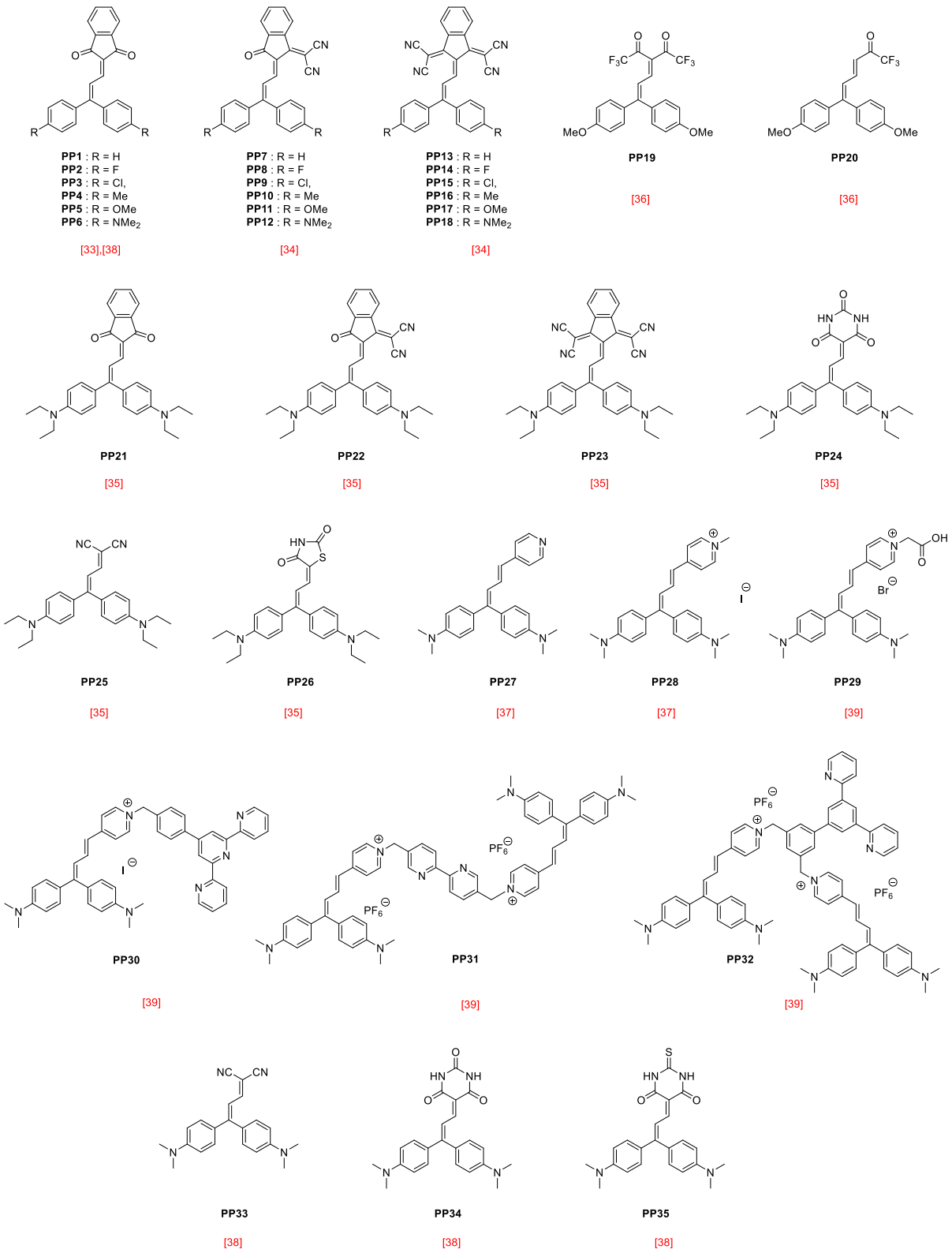

Figure 1. Chemical structures of dyes **PP1**-**PP35** reported in the literature.

To evidence the real electron-donating ability of the 4,4-*bis*(4-methoxyphenyl)butadienyl donor, comparisons with four dyes **PP6**, **D10**-**D12** differing from **PP5**, **PP11**, **PP17** and **D1**-**D9** by the electron donors have also been synthesized. Finally, to support the experimental results, theoretical calculations were carried out.

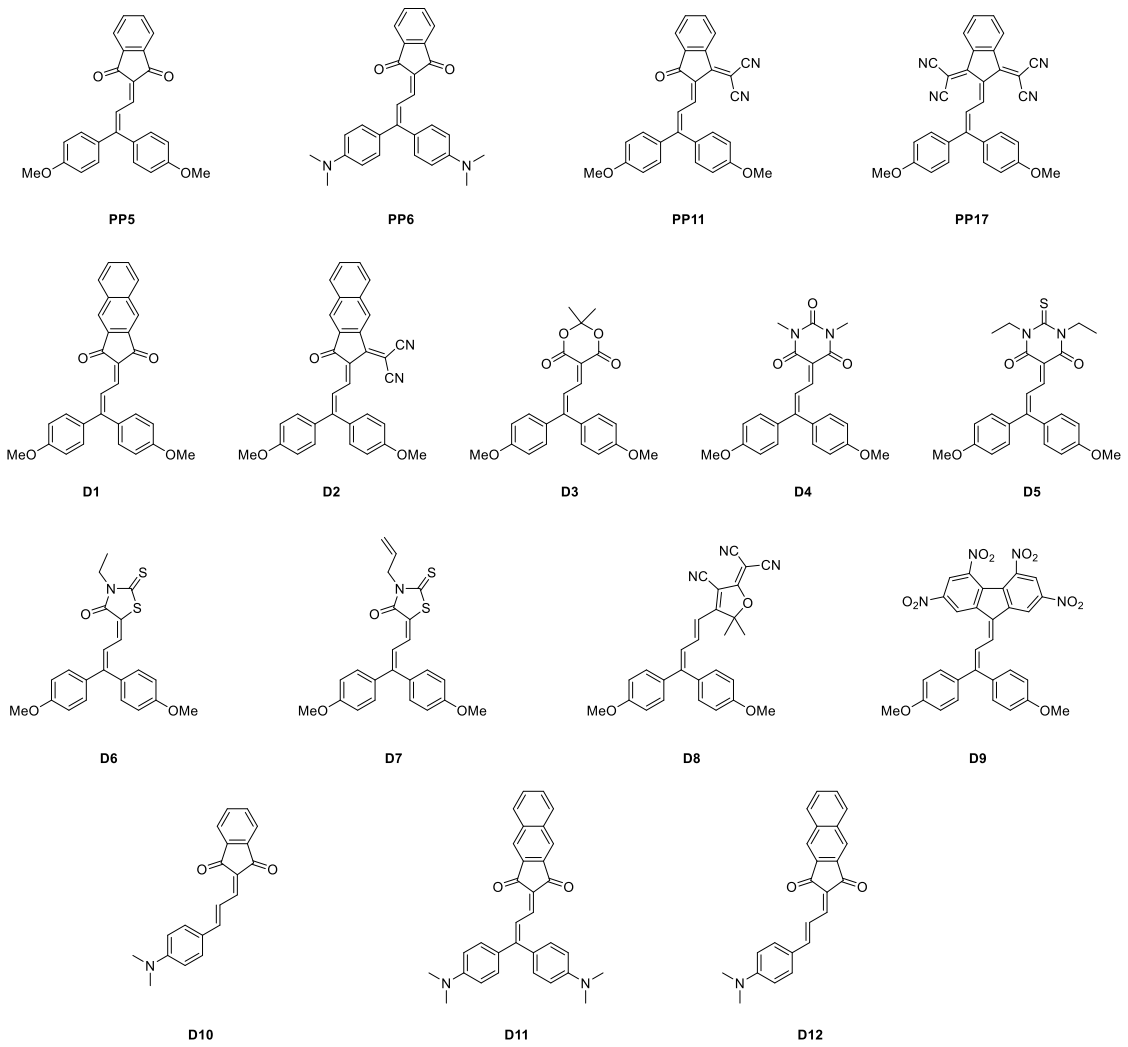

Figure 2. Chemical structures of the sixteen dyes **PP5**, **PP6**, **PP11**, **PP17** and **D1-D12** investigated in this work.

2. Results and Discussion

2.1. Synthesis of the dyes

The sixteen dyes **PP5, PP11** and **D1-D11** reported in this work have been synthesized using a standard method consisting in a Knoevenagel reaction. Even if this reaction was reported as soon as 1896 by Knoevenagel between benzaldehyde and ethyl acetoacetate in the presence of piperidine as the catalyst,[44] this latter was not adapted for the synthesis of dyes **PP11** and **D2** for which diisopropylethylamine (DIPEA) was used instead of piperidine. Indeed, as evidenced by recent reports in the literature, in the case of dyes based on 2-(3-oxo-2,3-dihydro-1*H*-inden-1-ylidene)malononitrile **EA2**, 2,2'-(1*H*-indene-1,3(2*H*)-diylidene) dimalononitrile **EA3** or extended analogues such as **EA5**, an unexpected cyclization reaction

can occur, resulting from the nucleophilic attack of the secondary amines onto the cyano groups, producing azafluorenones.[45-49] By opposing 3,3-*bis*(4-methoxyphenyl)acrylaldehyde **ED1**, Michler's aldehyde (3,3-*bis*(4-(dimethylamino)phenyl)acrylaldehyde) **ED2** or 3-(4-(dimethylamino) phenyl)acrylaldehyde **ED3** to the appropriate electron acceptors **EA1-EA12** in the presence of piperidine or DIPEA, the different dyes could be isolated in pure form with reaction yields ranging from 75% for **D3** to 92% for **PP11** respectively (See Scheme 1).

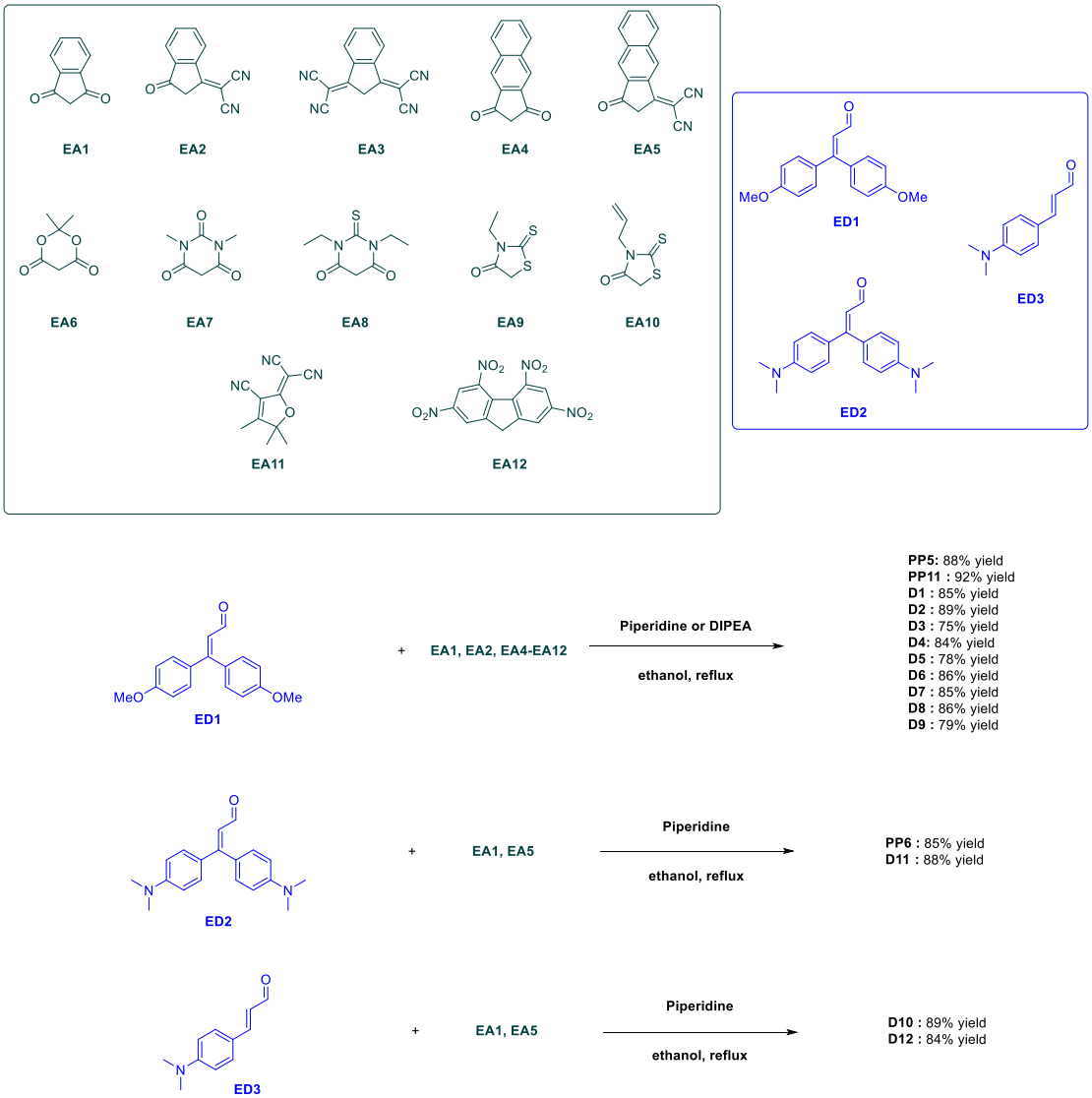

Scheme 1. Synthetic routes to the sixteen dyes **PP5, PP11** and **D1-D11** reported in this work.

Finally, due to the remarkable stability of the **EA3** anion in basic conditions, condensation of **EA3** on **ED1** could not be carried in these conditions and the Knoevenagel reaction could only been carried out in acidic conditions, in this case acetic anhydride. At the end, **PP17** could be isolated in pure form in 94% yield.

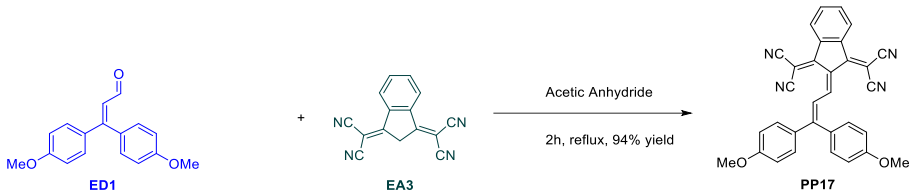

Scheme 2. Synthetic route to **PP17**.

It has to be noticed that among the twelve electron acceptors used in this study, **EA2**,[50] **EA3**,[51] 1*H*-cyclopenta[*b*]naphthalene-1,3(2*H*)-dione **EA4**,[52] 2-(3-oxo-2,3-dihydro-1*H*-cyclopenta[*b*] naphthalen-1-ylidene)malononitrile **EA5**,[45,53] 2-(3-cyano-4,5,5-trimethylfuran-2(5*H*)-ylidene) malononitrile **EA11**[54] and 2,4,5,7-tetranitro-9*H*-fluorene **EA12**[55-56] have been prepared according to procedures previously reported in the literature. The different dyes (except **PP17**) were also synthesized in ethanol which is a biosourced solvent so that the concepts of Green Chemistry have been applied to their syntheses. All dyes could be obtained in pure form by simple filtration on a glass filter, which is the simplest procedure to purify compounds. Among the series of 16 dyes examined in this work, only 7 of them (**PP5**, **PP11**, **PP17, D1, D2, D10-D12)** have previously been reported in the literature, demonstrating the novelty and the systematic approach developed in this work.

Finally, by slow evaporation of chloroform, crystals could be obtained for several dyes, and their structures could be solved by single-crystal X-ray diffraction as exemplified with **PP5** and **PP17** (See Figure 3). It has to be noticed that in the crystal structure of **PP17**, a co-crystallization with chloroform molecules could be clearly evidenced. As shown in the Figure 3, a fully planar structure could be found between the electron donor and the electron-accepting moiety, optimizing the electronic delocalization between the two partners. However, a torsion angle can be found between one of the aromatic rings of the electron-donating group and the rest of the structure. Thus, an angle of 73.3° could be determined for **PP5** whereas this angle increased up to 75.1° in **PP17**. The higher deviation found in **PP17** can be assigned to the steric hindrance generated by the dicyanovinylene group, enforcing a rotation of one of the aromatic rings. Conversely, in the case of **PP5**, a reduced steric hindrance exists between the oxygen atom of the acceptor and the methoxyphenyl group so that a reduced dihedral angle could be determined. Interestingly, a drastic influence on the planarity of the structure could be found. Thus, if the electron donor is almost coplanar with the electron donor in **PP5** (dihedral angle between the donor and the acceptor being of 178.975(55)°, conversely, for **PP17**, an angle of 147.918(104)° could be found between the two partners. Even if the lack of planarity of this structure should influence the optical properties and the electronic delocalization of the

structure, the latter detailed optical properties will reveal that the lack of planarity could not dramatically impact the optical properties, the position of the intramolecular charge transfer (ICT) band of this dye being correctly positioned, with regards to the electron withdrawing ability of **EA3** and that of the other electron acceptors.

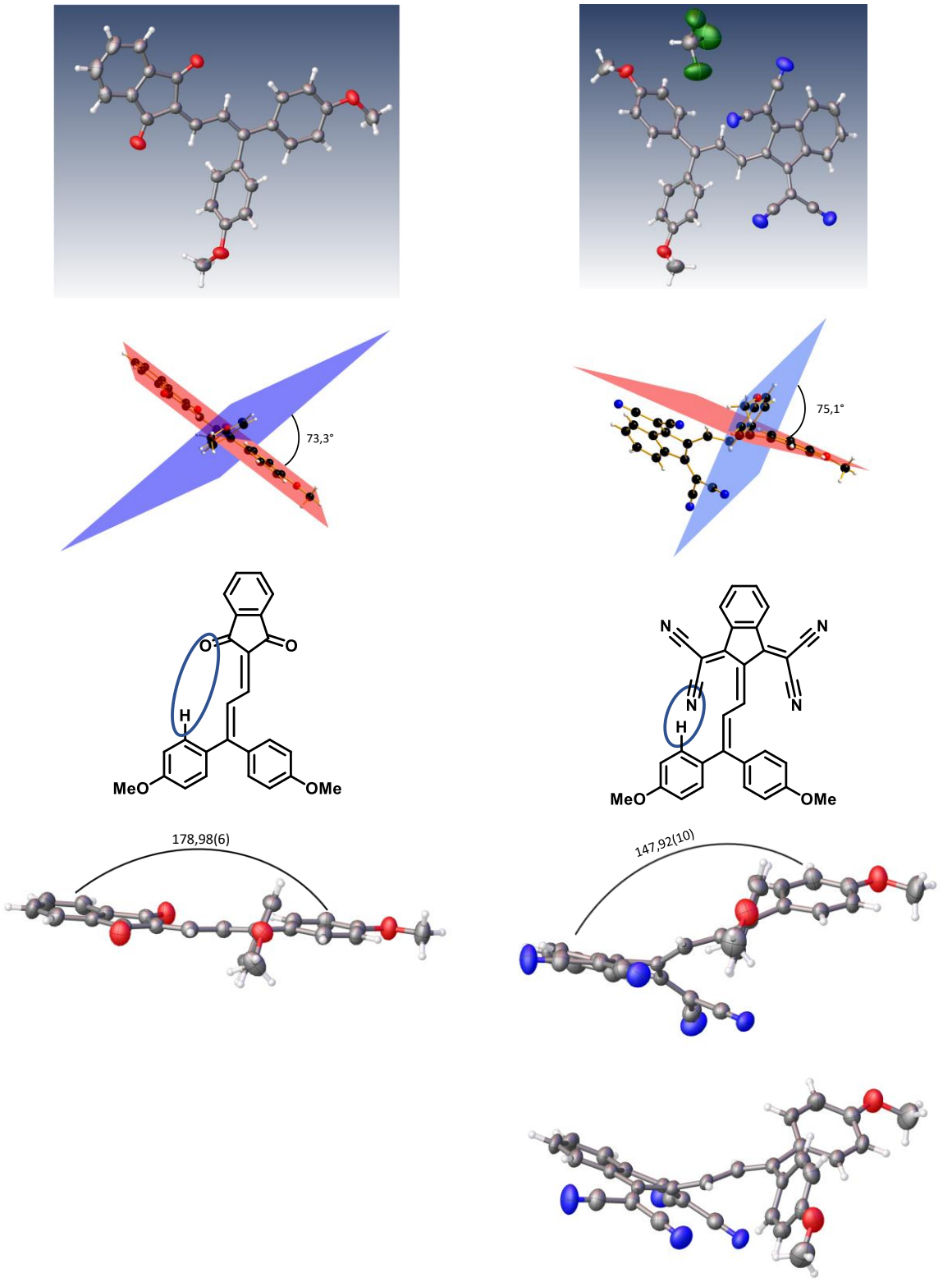

Figure 3. Crystal structures of **PP5** (CCDC 2065156) and **PP17** (CCDC 2065157).

2.3. Theoretical calculations

The B3LYP/6-311G(d,p) level of theory using Gaussian 09 program have been used for geometry optimization and also for the calculation of the Highest Occupied Molecular Orbital (HOMO) and the Lowest Unoccupied Molecular Orbitals (LUMO) energy levels in chloroform.[57-63] As anticipated, use of a similar electron donor (**ED1**) in all dyes furnished HOMO orbitals of similar energy levels and with a similar electronic distribution (See Table 1 and Figure 4). On the opposite, a greater modification of the LUMO energy levels could be found, consistent with a modification of the electron-withdrawing abilities of **EA1-EA12**. By examining the contour plots of the HOMO and LUMO orbitals for **PP5**, **PP11**, **PP17**, **D1-D9**, a HOMO orbital located on the 4,4-*bis*(4-methoxyphenyl)butadienyl moiety and a LUMO orbital centered onto the electron acceptor confirmed that the HOMO-LUMO gaps in **PP5**, **PP11**, **PP17**, **D1-D9** only varied by the position of the LUMO level.

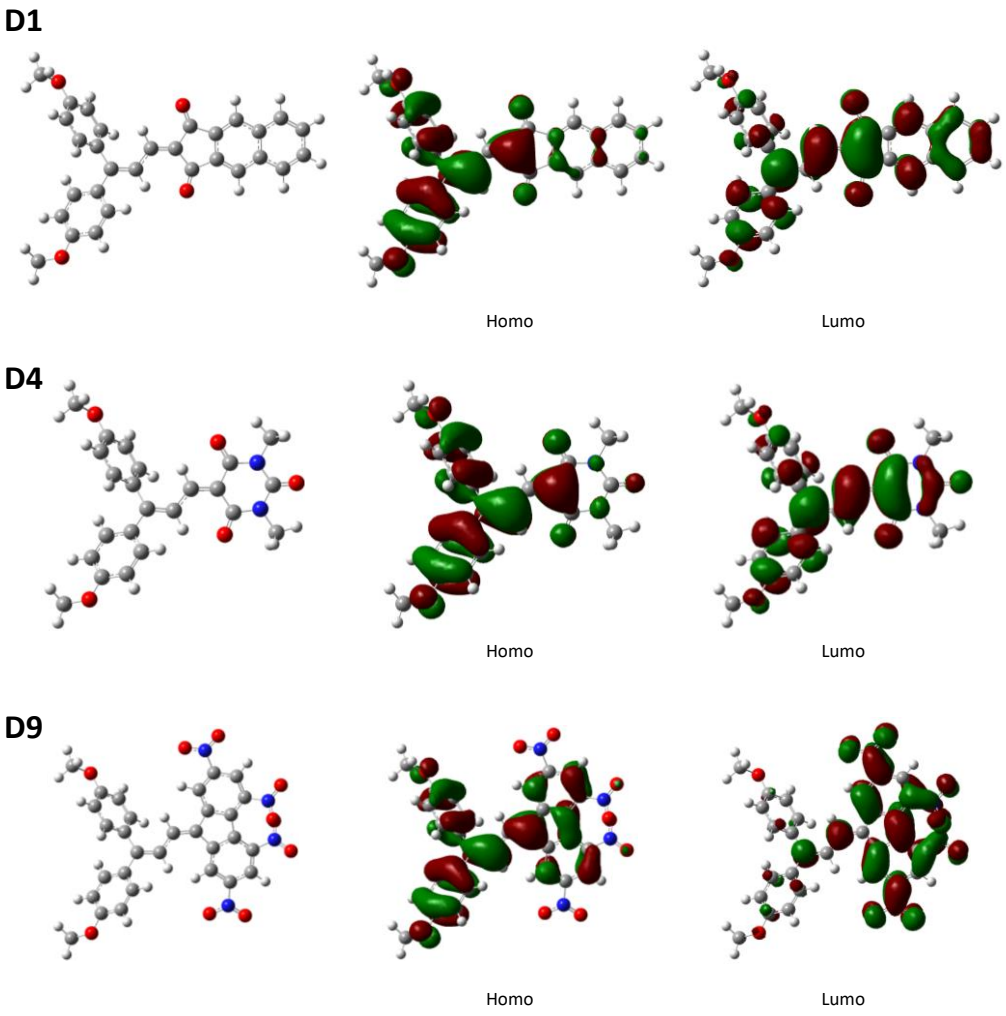

Figure 4. Optimized geometries and HOMO/LUMO electronic distributions of **D1, D4** and **D9**.

Also, to get a deeper insight into the transitions involved in the visible range, DFT calculations were performed using the same model. Chloroform was selected as the solvent and the polarizable continuum model (PCM) was selected as the solvent model for the TD-DFT calculations. A dielectric constant of 4.9 was used for the calculations. The theoretical UV-visible absorption spectra are presented in the Figure 5. A comparison between the theoretical and the experimental UV-visible absorption spectra is provided in the next paragraph.

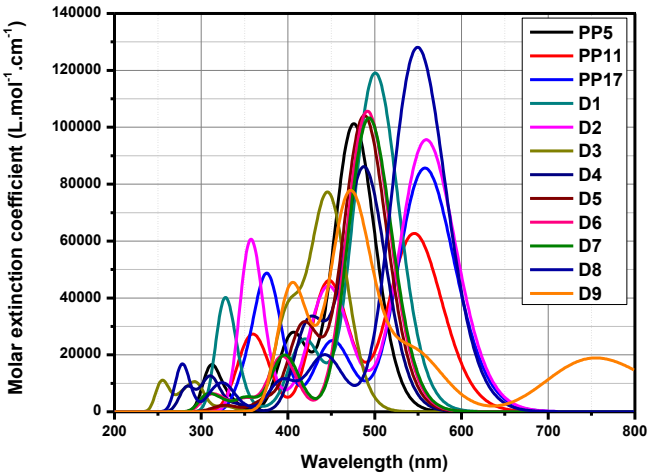

Figure 5. Simulated absorption spectra in dilute chloroform of synthetized compounds **PP5**, **PP11**, **PP17**, **D1-D9**.

Table 1. Summary of the simulated absorption characteristics in dilute chloroform of the different compounds. Data were obtained in chloroform solutions.

Compounds	E_{HOMO} (eV)	E_{LUMO} (eV)	λ_{max} (nm)	Transitions
D1	-5.97	-3.12	498	HOMO->LUMO (99%)
			436	HOMO-3->LUMO (88%)
			422	HOMO-1->LUMO (97%)
			414	HOMO-2->LUMO (90%)
D2	-6.01	-3.44	558	HOMO->LUMO (99%)
			464	HOMO-1->LUMO (88%)
			451	HOMO-2->LUMO (98%)
			433	HOMO->LUMO+1 (83%)
			407	HOMO-4->LUMO (85%)
D3	-6.11	-2.97	445	HOMO->LUMO (97%)
D4	-6.05	-2.99	457	HOMO->LUMO (98%)
D5	-6.06	-3.15	512	HOMO-1->LUMO (93%)
			486	HOMO->LUMO (94%)

			414	HOMO-2-> LUMO (98%)
D6	-5.72	-2.89	490	HOMO->LUMO (99%)
			435	HOMO-1->LUMO (90%)
D7	-5.74	-2.91	492	HOMO->LUMO (99%)
			438	HOMO-1->LUMO (87%)
D8	-6.02	-3.45	546	HOMO->LUMO (99%)
			437	HOMO-1->LUMO (99%)
D9	-6.05	-3.94	733	HOMO->LUMO (99%)
			536	HOMO->LUMO+1 (97%)
			508	HOMO-1->LUMO (94%)
			490	HOMO->LUMO+2 (93%)
			467	HOMO->LUMO+3 (97%)
			449	HOMO->LUMO+4 (97%)
			415	HOMO-2->LUMO (94%)
			411	HOMO-1->LUMO+1 (87%)
D10	-5.55	-2.94	533	HOMO->LUMO (100%)
			442	HOMO->LUMO+1 (98%)
			411	HOMO-2->LUMO (52%), HOMO-1->LUMO (43%)
D11	-5.41	-2.90	569	HOMO->LUMO (93%)
			527	HOMO-1->LUMO (92%)
			424	HOMO-4->LUMO (39%), HOMO-3->LUMO (56%)
			422	HOMO->LUMO+1 (86%)
			402	HOMO-2->LUMO (88%)
D12	-5.57	-3.07	561	HOMO->LUMO (100%)
			432	HOMO-2->LUMO (79%)
			422	HOMO-1->LUMO (56%), HOMO->LUMO+1 (42%)
			409	HOMO-1->LUMO (43%), HOMO->LUMO+1 (56%)
PP5	-5.97	-3.00	474	HOMO->LUMO (98%)
			415	HOMO-2->LUMO (81%), HOMO-1->LUMO (14%)
			402	HOMO-1->LUMO (65%), HOMO->LUMO+1 (21%)
PP6	-5.39	-2.76	541	HOMO-1->LUMO (11%), HOMO->LUMO (89%)
			507	HOMO-1->LUMO (88%), HOMO->LUMO (11%)
			448	HOMO->LUMO+1 (98%)
			404	HOMO-3->LUMO (69%), HOMO-2->LUMO (25%)
PP11	-6.04	-3.35	543	HOMO->LUMO (97%)
			451	HOMO->LUMO+1 (91%)
			436	HOMO-1->LUMO (96%)
PP17	-6.08	-3.47	569	HOMO->LUMO+1 (96%)
			557	HOMO->LUMO (99%)
			450	HOMO-1->LUMO (98%)
			431	HOMO-1->LUMO+1 (99%)

2.2. Optical properties

Push-pull dyes, which consists in structure combining an electron donor connected to an electron acceptor by mean of a π-conjugated spacer, are characterized by an intense absorption band in the visible range corresponding to the intramolecular charge transfer (ICT) band. Considering that **PP5**, **PP11**, **PP17**, **D1-D9** are soluble in chloroform, their UV-visible absorption properties were examined in this solvent. As shown in the Figure 6, a strong absorption band can be detected in the visible range for all dyes, with absorption maxima ranging from 439 nm for **D3** bearing the weakest electron acceptor **EA6** to 500 nm for **PP17** and 553 nm for **D2**, substituted with the strongest electron acceptors **EA3** and **EA5** respectively. Two groups of dyes can be distinguished. Thus, a first group of dyes absorbing between 435 and 460 nm can be identified, comprising **PP5**, **D3**, **D4**, **D6** and **D7**. This first family of dyes comprises weak acceptors such as indane-1,3-dione **EA1**, Meldrum acid **EA6**, *N*-methylbarbituric acid **EA7** or rhodanines **EA9** and **EA10**. In the second group, dyes such as **PP11**, **PP17**, **D2**, and **D8** can be identified, possessing **EA2**, **EA3**, **EA5** and **EA11** as acceptors. Considering that the 12 dyes have been prepared with the same electron donor, **EA3** and **EA5** are undoubtedly the most electron-accepting groups of the series. Interestingly, a perfect overlap of the ICT bands of **D1** and **D5** was also detected in chloroform (See Figure 6a), demonstrating that the electron-withdrawing abilities of **EA5** and **EA8** are rather similar. The same conclusions can also be done while comparing the ICT bands of **PP17** and **D2** bearing **EA3** and **EA5** as acceptors. Considering that **EA5** is only substituted with two cyano groups, its conversion as a tetracyano-substituted acceptor (as done for **EA3**) could produce an exceptional electron acceptor. However, all attempts to get this electron acceptor failed. Finally, the most intriguing acceptor of the series was **EA12**. By using this electron acceptor, a compound (**D9**) exhibiting two ICT bands could be obtained, with the two maxima located at 469 and 553 nm. **D9** showed a broad absorption band extending from the UV to the visible range, namely from 350 nm to 700 nm (See Figure 6b). Based on previous works aiming at examining the specificities of the UV-visible absorption spectra of 2,4,5,7-tetranitrofluorene-based push-pull dyes, the absorption band located at long-wavelength can be assigned to an electron density transfer along the axis of the molecule from the donor to the electron-withdrawing fluorene moiety.[64] This band is considered as being the ICT band of the dye. Conversely, at short wavelength, this band was determined as originating from an electron density transfer from atoms adjacent to the polymethine chain and the nitro groups of the

fluorene acceptor. This band was determined as corresponding to the polymethine nature of the absorption band.

Finally, to position **ED1** with regards to the other electron donors, a comparison was established with dyes based on **ED2** and **ED3**. For this purpose, **PP6**, **D10-D12** were synthesized, enabling a comparison with dyes comprising two different electron acceptors, **EA1** and **EA4**. As shown in the Figures 6c and 6d, a similar trend was found for the two series **PP5**, **PP6** and **D1**, **D10**, **D11** and **D12** respectively, except that a red-shift was observed of the absorption maxima was found for the second series (**D1**, **D11** and **D12**), consistent with an improvement of the electron-withdrawing ability in **EA4**. Compared to **D10** and **D12**, a redshift as high as 200 nm was found for the absorption maxima of **PP5** and **D1**, evidencing the weak electron donating ability of **ED1**.

a)

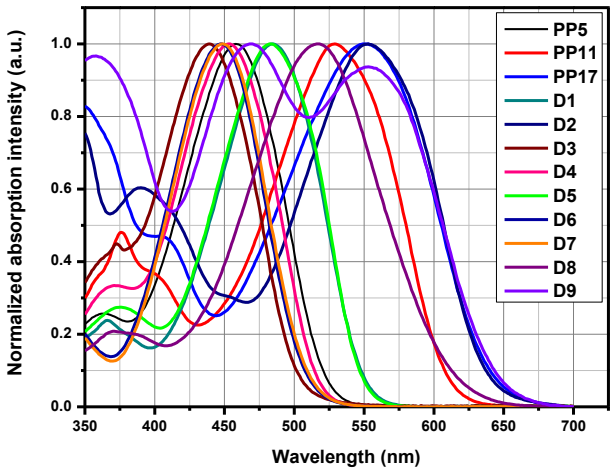

b)

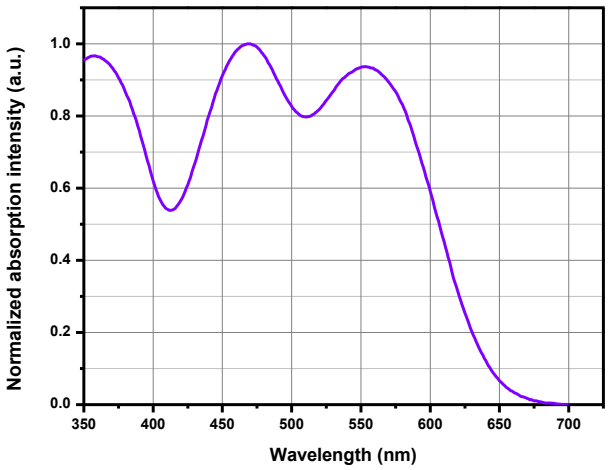

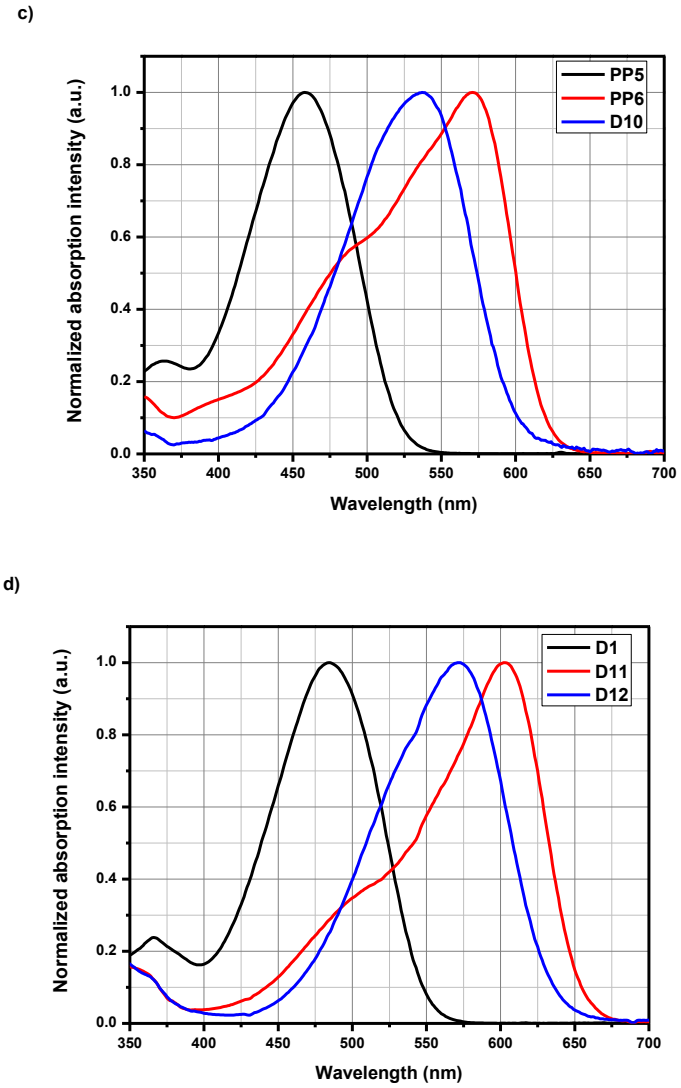

Figure 6. Normalized UV-visible absorption spectra in chloroform of a) **PP5**, **PP11**, **PP17**, **D1**-**D9**, b) **D9**, c) **PP5**, **PP6** and **D10**, d) **D1**, **D11** and **D12**.

Examination of their molar extinction coefficients (See Figure 7a and Table 2) revealed **PP5**, **D4** and **D7** to exhibit the highest molar extinction coefficients of the series, peaking at 49 500, 46 200 and 52 000 $M^{-1}.cm^{-1}$ respectively. Besides, these values remain far behind that of the reference compounds **D11** and **D12** for which molar extinction coefficients close to 77 000 $M^{-1}.cm^{-1}$ could be determined (See Figure 7b). The crystal structures have also revealed that the π-conjugated system of **PP5** was fully planar contrarily to that observed in **PP17** for which a slightly incurved π-conjugated system was found. Besides, with regard to the absorption maxima (458 and 550 nm for **PP5** and **PP17** respectively), no detectable influence on the electronic delocalization can be detected between these two dyes. Indeed, **EA3** is a

stronger electron acceptor than **EA1**, supporting the redshift of the ICT band of **PP17** by ca. 100 nm compared to that of **PP5**.

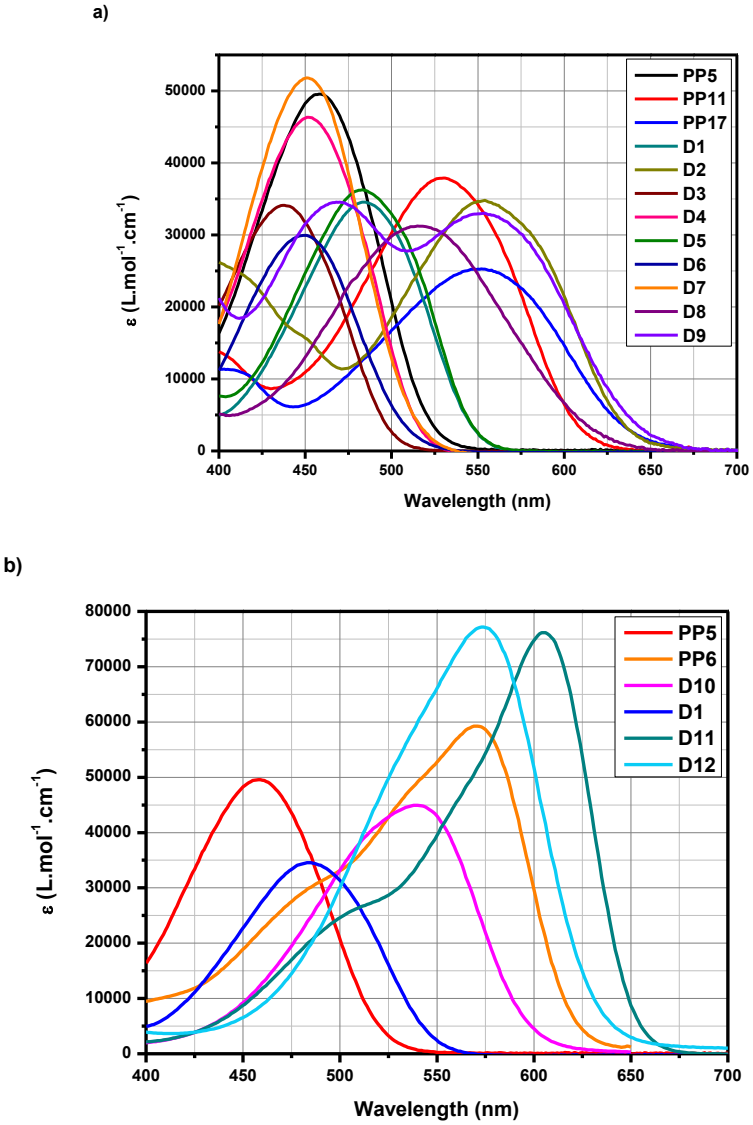

Figure 7. UV-visible absorption spectra in chloroform of a) **PP5**, **PP11**, **PP17**, **D1-D9**, b) a series of selected dyes **PP5**, **PP6** and **D10**, d) **D1**, **D11** and **D12.**

Table 2. Optical characteristics of the different compounds in chloroform and the values theoretically determined.

chloroform								
compounds	**PP5**	**PP6**	**PP11**	**PP17**	**D1**	**D2**	**D3**	**D4**
λ (nm)	458	571	530	550	484	552	429	452
ϵ ($M^{-1}.cm^{-1}$)	49300	59400	37800	25000	34600	34800	34100	46300
Δ E(eV)	2.71	2.17	2.34	2.25	2.56	2.25	2.89	2.74
compounds	**D5**	**D6**	**D7**	**D8**	**D9**	**D10**	**D11**	**D12**
λ (nm)	482	447	449	517	469, 554	539	606	574

ϵ ($M^{-1}.cm^{-1}$)	36300	30000	51700	31400	34500, 32600	44800	76000	77100
Δ E(eV)	2.57	2.77	2.76	2.40	2.24	2.30	2.04	2.16

Theoretical values in chloroform								
compounds	**PP5**	**PP6**	**PP11**	**PP17**	**D1**	**D2**	**D3**	**D4**
λ (nm)	474	528	542	557	499	558	444	458
ϵ ($M^{-1}.cm^{-1}$)	101000	116600	64300	85500	118600	95100	76700	86260
Δ E(eV)	2.62	2.35	2.29	2.23	2.48	2.22	2.79	2.71
compounds	**D5**	**D6**	**D7**	**D8**	**D9**	**D10**	**D11**	**D12**
λ (nm)	486	490	491	546	468, 545	533	542	560
ϵ ($M^{-1}.cm^{-1}$)	105000	106500	103700	128800	72200,22400	97800	64300	111452
Δ E(eV)	2.55	2.53	2.52	2.27	2.27	2.33	2.29	2.21

As experimentally observed, positions of the ICT bands of **PP5**, **PP11**, **PP17**, **D1-D9** are clearly redshifted by increasing the electron withdrawing ability of the acceptors. The most red-shifted absorptions are detected for **PP17**, **D2** and **D9**. A good agreement between the theoretical positions of the ICT bands with those of the experimental ones can be detected. Notably, to illustrate this, **PP17**, **D2** and **D9**, an error lower than 10 nm can be determined, the experimental ICT bands being located at 550, 552 and 554 nm vs. 557, 558 and 545 nm respectively for the theoretical ones. A good agreement between the theoretical and the experimental HOMO-LUMO gaps were also found, the experimental and the theoretical UV-visible spectra being both determined in chloroform. Interestingly, comparisons of the experimental and theoretical values of HOMO-LUMO gaps revealed the theoretical ones to be underestimated, except for **PP6** and **D11** for which the opposite situation was found. As specificity, the two dyes are based on indane-1,3-dione **EA1** and 1*H*-cyclopenta[*b*]naphthalene-1,3(2*H*)-dione **EA4** as the electron acceptors, that are two acceptors only differing by their polyaromaticities. Only a good agreement between the theoretical and the experimental values was found for **D10** and **D12** that also bear **EA1** and **EA4** as the electron acceptors. Clearly, differences between the theoretical and the experimental HOMO-LUMO gaps rely in parameters that are not correctly considered during the calculations such as the internal torsion of the molecules. As shown by the crystallographic structures, one of the two aromatic tings of the electron donating group exhibit a severe deviation relative to the average plane of the molecules due to steric hindrance generated by the electron accepting groups. Contribution of this aromatic ring is not correctly taken into account during the theoretical calculations. Since the same electron donor is used for the design of all dyes (**PP5**, **PP11**, **PP17**, **D1-D12)**, variations of the HOMO-LUMO gap only depends on a modification of the position of the LUMO levels. To evidence this, electronic distribution of the HOMO and LUMO orbitals of **PP5**, **PP11**, **PP17**, **D1-D12** was investigated. This part is detailed in the previous section. A

summary of the main transitions involved in the theoretical UV-visible absorption spectra is provided in the Table 1.

As anticipated for push-pull dyes, the transition detected at the lowest energy mainly arises from a HOMO-> LUMO transition. Parallel to this, in the case of **D5**, a HOMO-1-> LUMO transition and a HOMO-> LUMO+1 transition for **PP17** were determined as the main transitions contributing to the ICT bands. For the transitions at higher energies, an admixture of transitions between HOMO-3, HOMO-2, HOMO-1 -> LUMO, LUMO+1, LUMO+2, LUMO+3 and even LUMO+4 could be determined, depending on the dye. A clear trend can be observed in this series of dyes: When the electron accepting properties of the acceptor part increase, a clear redshift is obtained for the ICT transition.

Within this series of dyes, the values of E_{LUMO} importantly varied as a function of the electron accepting ability of the acceptor part whereas the values of E_{HOMO} slightly changed. These results are in accordance with the fact that the same electron donor has been used in these different dyes and that only the electron acceptors varied. Finally, as mentioned earlier, **D9** which possesses TNF as the electron accepting group exhibits two ICT bands detected at 469 and 554 nm respectively. As shown in the Figure 8, several optical transitions are theoretically predicted in the visible range. Besides, the transition predicted at 740 nm in chloroform or 770 nm in acetonitrile was not observed in the experimental UV-visible absorption spectrum. However, two transitions are predicted at higher energy, notably, at 475 and 558 nm in chloroform, 470 and 560 nm in acetonitrile, that fit to the two experimental transitions detected at 469 and 554 nm in chloroform. Based on the theoretical calculations, these two absorption bands are assigned to HOMO-1 -> LUMO and HOMO-> LUMO+1 transitions.

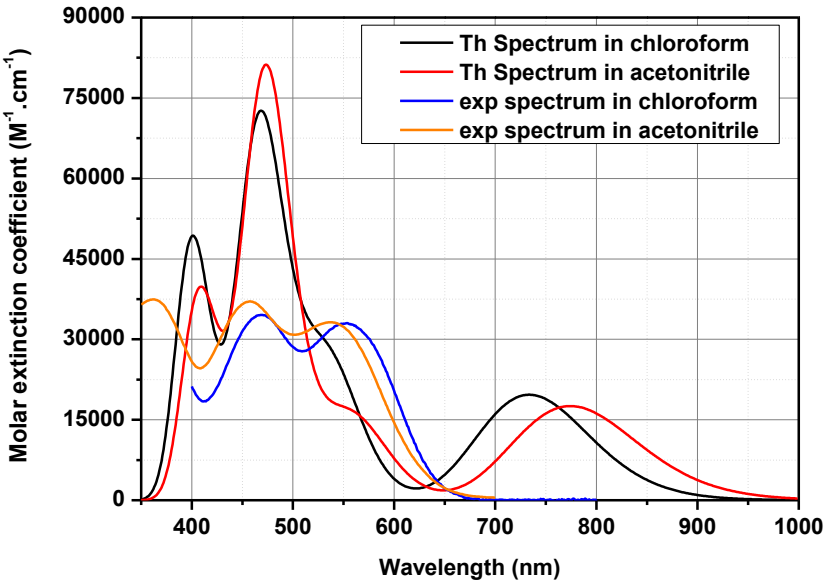

Figure 8. Theoretical and experimental UV-visible absorption spectra of D9 in chloroform and acetonitrile.

2.4. Solvatochromism

As evidenced in the previous paragraphs, major differences of the position of the absorption maxima can be found between the different dyes in chloroform, resulting from a modification of the electron accepting groups (**EA1-EA12**). To get a deeper insight into the absorption properties of **PP5**, **PP11**, **PP17**, **D1-D9**, their solvatochromic behaviors were examined in 23 solvents of different polarity. A summary of the absorption properties is provided in the Tables 3 and 4. As displayed in these tables, a variation of the positions of the absorption maxima can be clearly evidenced, corresponding to a solvatochromic behaviour. To evidence the intramolecular nature of the charge transfer, dilutions of the solutions were carried out, and a linear decrease of the absorbance vs. the concentration could be obtained for the different dyes. To rationalize the variation of positions of the ICT bands, several solvatochromic scales have been tested, as exemplified by the Kamlet-Taft's,[65] Dimroth-Reichardt's,[66] Lippert-Mataga's,[67] Catalan's,[68-69] Kawski-Chamma-Viallet's,[70] McRae's,[71] Suppan's,[72] Bakhshiev's [73] scales. In these different scales, the polarity and/or the polarizability of the solvents are considered, through parameter such as the solvent polarity parameter $E_T(30)$ for the Reichardt's scale, the solvent polarizability (SP), the solvent dipolarity (SdP) and the solvent polarity/polarizability (SPP) parameters of the Catalan scales. Parallel to this, Taft parameters π^* is indicative of the ability of the solvents to stabilize a charge or a dipole by virtue of electric dielectric effects.[64] If the Lippert Mataga scale examines the solvatochromism as a function of the orientation polarizability, the dipole moment and the

refractive index *n* of solvents, McRae developed an improved version of the Lippert-Mataga scale by additionally taking into account the solute polarizability for dyes.[67,71] Conversely, the Bakhshiev's, Kawaski-Chamma-Viallet scales examine the variation of excited state dipole moments as a function of the static dielectric constant (ε_r) and the refractive index *n* of the solvents. Irrespective of the empirical scales, straight lines should be obtained while plotting the different graphs, if the selected scale is adapted to describe the solvatochromism.

Table 3. Optical properties of **PP5**, **PP11**, **PP17**, **D1-D9** in 23 solvents.

compounds	**π*[1]**	**PP5[2]**	**PP6[2]**	**PP11[2]**	**PP17[2]**	**D1[2]**	**D2[2]**	**D3[2]**	**D4[2]**
acetone	0.71	446	558	517	530	471	541	423	431
acetonitrile	0.75	446	558	509	525	468	541	423	432
AcOEt	0.54	444	542	517	530	467	540	418	431
anisole	0.73	455	563	536	544	479	551	432	440
butanol	0.47	461	578	525	556	483	552	435	447
chloroform	0.78	458	571	530	550	484	552	439	452
cyclohexane	0.00	435	525	516	534	459	534	415	429
1,2-dichloroethane	0.81	453	566	525	543	479	550	429	443
dichloromethane	0.82	453	568	527	542	478	549	433	445
diethyl carbonate	0.45	440	541	516	532	468	536	420	430
diethyl ether	0.27	440	527	517	534	461	535	417	430
diglyme	0.64	449	560	524	541	476	547	427	438
1,4-dioxane	0.55	446	540	516	535	471	537	421	432
dimethylacetamide	0.88	454	573	527	530	479	551	432	437
dimethylformamide	0.87	453	574	524	nd[3]	477	nd[3]	432	436
DMSO	1.00	457	581	526	535	483	551	437	441
ethanol	0.54	453	577	522	550	481	548	434	443
heptane	-0.08	434	521	512	533	455	533	411	427
nitrobenzene	1.01	460	583	538	551	486	562	441	450
THF	0.58	447	552	520	532	472	545	425	434
toluene	0.54	450	548	522	539	474	544	428	437
triethylamine	0.14	438	523	526	nd[3]	462	nd[3]	419	434
p-xylene	0.43	448	544	521	540	472	543	426	435

[1] Kamlet and Taft parameters [2] Position of the ICT bands are given in nm [3] nd : not determined

Table 4. Optical properties of **PP5**, **PP11**, **PP17**, **D1-D9** in 23 solvents.

compounds	**π*[1]**	**D5[2]**	**D6[2]**	**D7[2]**	**D8[2]**	**D9[2]**	**D10[2]**	**D11[2]**	**D12[2]**
acetone	0.71	468	438	439	499	538	526	595	562
acetonitrile	0.75	466	433	437	499	538	528	597	565
AcOEt	0.54	466	433	435	494	533	520	579	546
anisole	0.73	475	446	446	504	549	530	599	567
butanol	0.47	474	442	442	511	542	nd[3]	nd[3]	nd[3]
chloroform	0.78	482	447	449	517	554	539	606	574

cyclohexane	0.00	459	429	430	486	516	481	556	532
1,2-dichloroethane	0.81	476	444	445	517	550	536	603	567
dichloromethane	0.82	477	443	446	515	551	537	603	571
diethyl carbonate	0.45	464	433	434	487	525	510	575	542
diethyl ether	0.27	466	nd[3]	431	493	530	502	569	534
diglyme	0.64	474	431	422	503	544	524	593	567
1,4-dioxane	0.55	466	434	434	491	529	512	581	545
dimethylacetamide	0.88	475	446	447	505	551	543	608	577
dimethylformamide	0.87	474	446	446	511	546	541	609	579
DMSO	1.00	478	448	450	513	553	554	620	590
ethanol	0.54	476	439	441	514	535	nd[3]	614	581
heptane	-0.08	456	427	428	482	513	478	551	529
nitrobenzene	1.01	486	456	458	528	570	552	613	585
THF	0.58	469	440	440	502	539	518	587	555
toluene	0.54	471	440	442	496	531	520	582	553
triethylamine	0.14	nd[3]	432	432	487	522	489	559	533
p-xylene	0.43	470	439	438	496	531	522	580	547

[1] Kamlet and Taft parameters [2] Position of the ICT bands are given in nm. [3] nd : not determined

Among the different empirical scales used to examine the solvatochromism of **PP5**, **PP11**, **PP17**, **D1-D9**, the most adapted ones were determined as being the Catalan and the Kamlet-Taft's scales (See the different graphs in SI). For all the other scales, no straight lines could be obtained and only an aleatory dispersion of points could be obtained. These different graphs are not reported in SI. In the case of the Catalan solvent polarity/polarizability scale, linear correlations were parametrized with three different parameters, namely, the solvent polarizability (SP), the solvent dipolarity (SdP) and the solvent polarity/polarizability (SPP) parameters.[74-76] The different plots can be found in SI. Interestingly, if linear correlations with remarkable values for the square of the correlation coefficients (R^2) could be obtained for all dyes by plotting the absorption maximum *vs.* the SPP and the SdP parameters, less favorable correlations were determined with the solvent polarizability (SP) parameter. Indeed, a higher dispersion of points could be detected in the different graphs (See Figures in SI). Therefore, it can be concluded that the solvatochromism of **PP5**, **PP11**, **D1-D9** is more influenced by the polarity of the solvent than its polarizability. These results were confirmed by the remarkable linear correlations obtained with the Kamlet-Taft's solvent polarity scale (see linear regressions in SI). In several cases, good correlations could also be obtained with the Reichardt polarity scale and an illustration of this is provided in the Figure 9 for compound **D3**. In light of these results, it can be concluded that the polarity/polarizability of the solvent is the primary cause influencing the position of the ICT bands as it constitutes the basis of the Kamlet-Taft's solvent polarity scale or the Catalan scale while using the polarity/polarizability (SPP) parameter.

Besides, based on the linear regressions obtained with the Catalan SP parameter that showed lower values of the square of the correlation coefficient (R^2), it can also be determined that the polarizability strongly influences the solvatochromism. Indeed, the major difference between the SPP and SP parameters relies in the fact that polarity and polarizability are dissociated with the SP parameters, only the polarizability being considered with this parameter. Considering that the SPP parameters can't dissociate polarizability from polarity but that good linear correlations are obtained with the SP parameters that only take into account of the polarizability, it can be assumed that certainly the polarizability strongly contributes to the linear correlations obtained with the SPP parameters. Irrespective of the polarity scales, the negative slopes are indicative of a positive solvatochromism, meaning that a significant charge redistribution occurs upon excitation (See Figure 9).

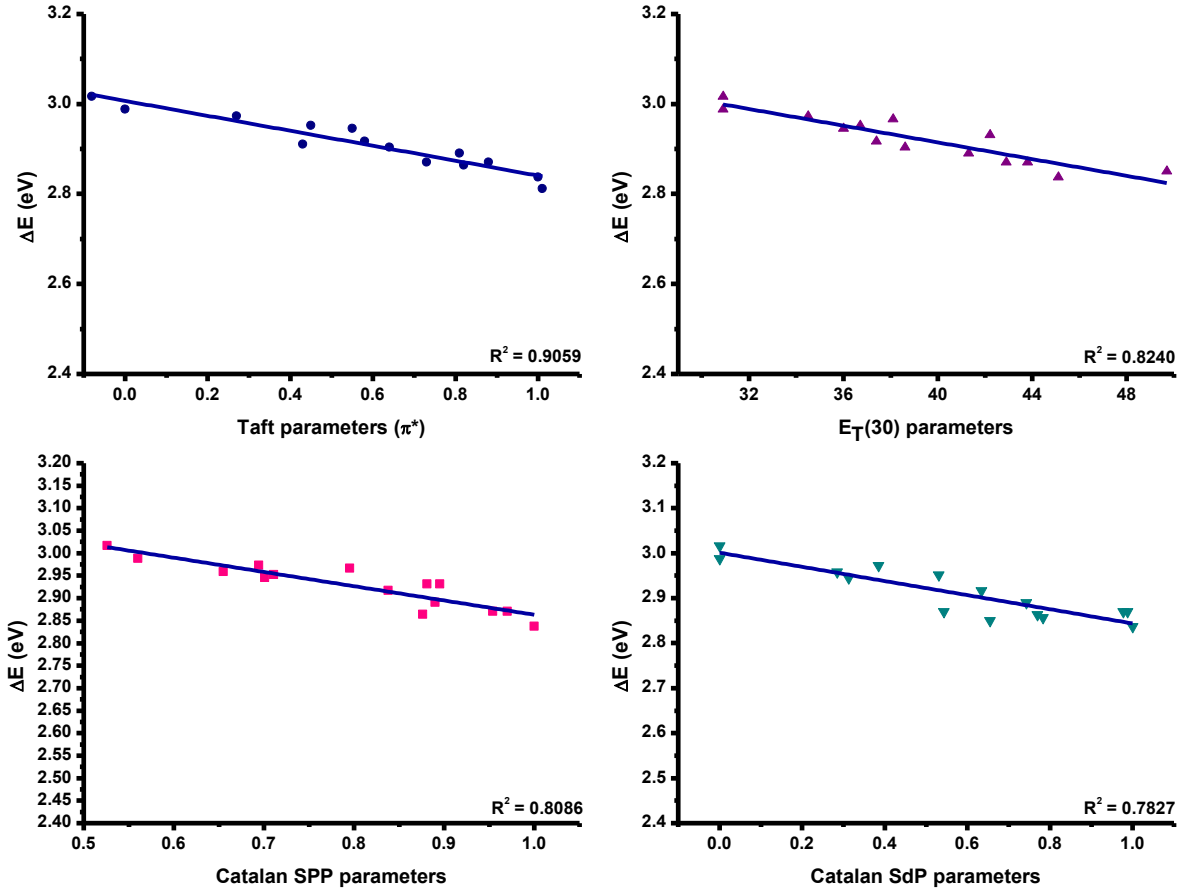

Figure 9. Linear correlations obtained while using four different polarity scales (Kamet-Taft, Catalan and Reichardt scales) for **D3**.

In this series, only one dye showed a solvatochromic behavior differing from the others, namely **PP17**. In this last case, lower linear regressions could be obtained while using the Catalan solvent polarizability (SP) with $R^2 = 0.708$ or the Reichardt scale ($R^2 = 0.657$) (See Figure 10). This atypical behaviour can be assigned to the presence of numerous CN groups on the electron acceptor enabling the create hydrogen bonds in high polar solvents. Consequently, the ability for **PP17** to create hydrogen bonds with the solvents becomes a primordial parameter, what is parametrized with the polarizability parameters.

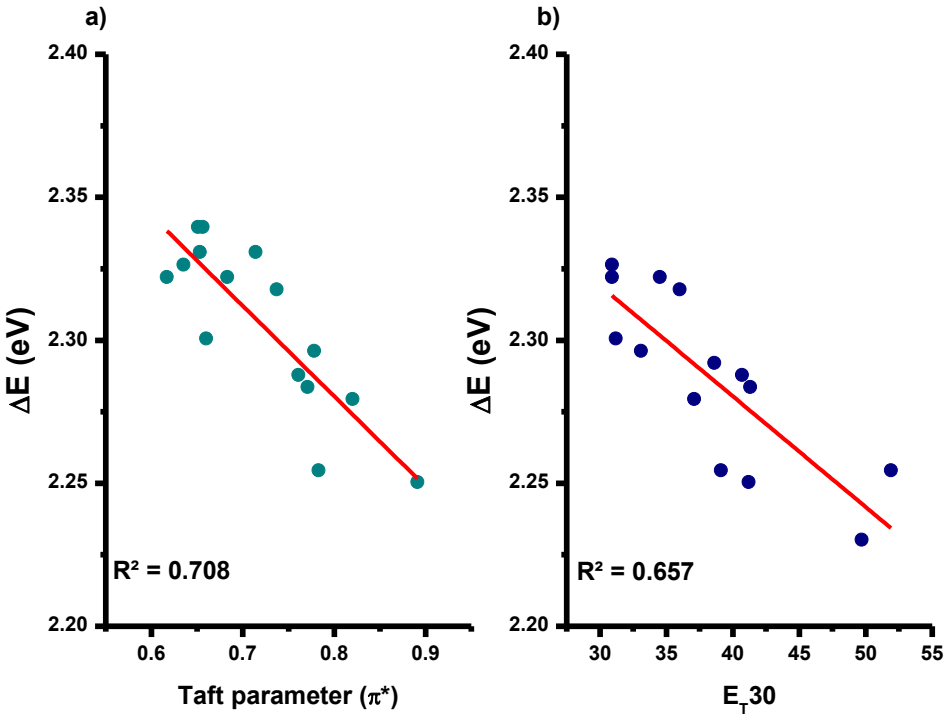

Figure 10. Linear correlations obtained for **PP17** while using a) the Kamlet-Taft parameter and b) the Reichardt (E_T30) parameter.

Interestingly, while examining the slopes obtained while plotting the HOMO-LUMO gap *vs.* the Kamlet-Taft parameter, similar slopes could be found for all dyes, demonstrating a similar sensitivity to the solvent polarity (See Figure 11).

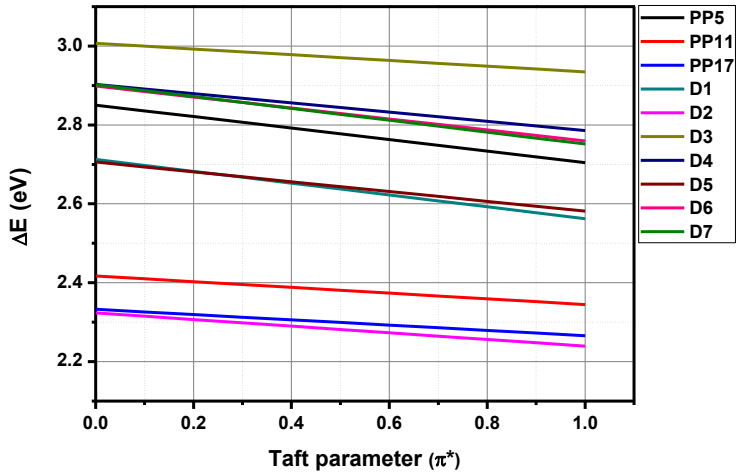

Figure 11. Variation of the positions of the charge transfer band with Kamlet-Taft empirical parameters.

Finally, solvatochromic properties of the references dyes **PP6**, **D10-D12** bearing other electron-donating groups than the 4,4-*bis*(4-methoxyphenyl)butadienyl donor was also examined. In this last case, the best correlations were obtained with the Kamlet-Taft parameters, enabling to get for the squares of the correlation coefficient (R^2), values ranging between 0.89 for **D12** to 0.98 for **D11** (See Figure 12). This is directly related to the higher electron donating ability of **ED2-ED4**, enabling to give rise to a higher electronic redistribution upon excitation. Finally, examination of the sensitivity to the solvent polarity revealed **PP6**, **D10-D12** to exhibit more negative slopes than the former series (See comparisons between **PP6**, **D10-D12** and **PP11** in Figure 13), consistent with the previous conclusions establishing a higher sensitivity to the solvent polarity. Indeed, due to the stronger electron donating groups used to prepare these dyes, a higher sensitivity to the environment and thus the polarity of the solvents can be observed for **PP6**, **D10-D12**, resulting in higher shifts of the ICT positions. Variation of the slopes is also related to the molecular structure. Indeed, the largest slopes were obtained for **PP6**, **D10**, **D11** and **D12**, all with the stronger dimethylamino donor moiety. Besides, no direct correlation with the dipole moment of the molecule can be established. Indeed, as shown in the Table 5, **PP6**, **D10**, **D11** and **D12** do not exhibit the largest dipole moments of the series of dyes. Indeed, in this field, **D8** clearly outperforms the other dyes, with a dipole moment of 20.18 D.

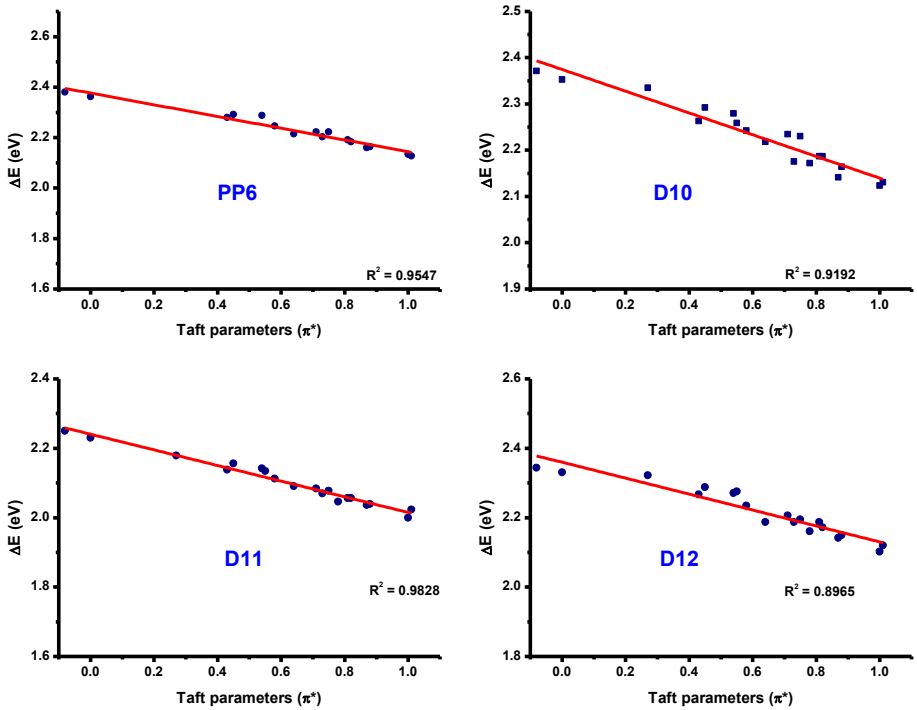

Figure 12. Linear correlations obtained while using the Kamet-Taft solvent polarity scale.

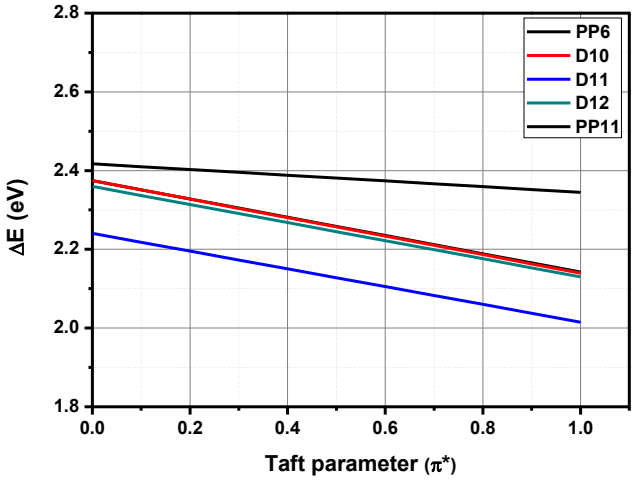

Figure 13. Variation of the positions of the charge transfer band with Kamlet-Taft empirical parameters for **PP11**, **D10-D12**.

Table 5. Dipole moment of the different dyes.

Compound	**PP5**	**PP6**	**PP11**	**PP17**	**D1**	**D2**
dipole moment	5.09	7.30	7.99	11.12	4.72	7.23
Compound	**D3**	**D4**	**D5**	**D6**	**D7**	**D8**
dipole moment	7.26	8.14	9.44	8.21	6.97	20.18

Compound	**D9**	**D10**	**D11**	**D12**		
dipole moment	16.56	5.45	7.30	5.16		

2.5. Electrochemical properties

Cyclic voltammetry (CV) has been used to investigate the electrochemical properties of all compounds either in diluted solutions of acetonitrile or in dichloromethane, in function of the solubility of the compounds in acetonitrile. All solutions were deaerated with argon for 10 min before any CV measurements. The redox potentials of all compounds are given against the half wave oxidation potential of the ferrocene (Fc)/ferrocenium cation couple and the different redox potentials are summarized in the Table 6. Along with the redox values are given the HOMO and LUMO energy levels of the different push-pull molecules determined by using as a standard the oxidation potential of Fc, based on the Pommerehne et al. calculations (4.8 eV vs. vacuum).[77]

The dyes were all designed using the same electron-donating group (**ED1**) which is the reason why almost similar oxidation potentials around 950 mV can be noticed for all dyes. Also, all the oxidation processes are irreversible, corresponding to one electron loss of the central double bound, except in the case of **PP17** where a slight reversibility was observed, showing that the acceptor, **EA3** which is the strongest electron acceptor of the series might certainly have a small impact on the oxidation process. Furthermore, two exceptions could be found in this set of compounds: **D6** and **D7** have much lower oxidation potentials than the other push-pulls, about 200 mV less compared to the others, as shown in Figure 14. These two compounds are composed of rhodanine moieties as the electron accepting groups and the DFT calculations have clearly established a high electronic density on the sulfur atoms. An oxidation of these sulfur atoms at lower potentials than the central double bond is then highly probable. Nevertheless, **D5** which comprises a thiobarbituric-based electron accepting group also possesses a sulfur atom in its scaffold. However, due to the higher electronic density on this atom in **D5** than in **D6** and **D7,** this atom can only be oxidized at much higher potentials. For this reason, **D5** oxidizes close to the oxidation potentials of the other dyes with a one irreversible electron process at 1.02V.

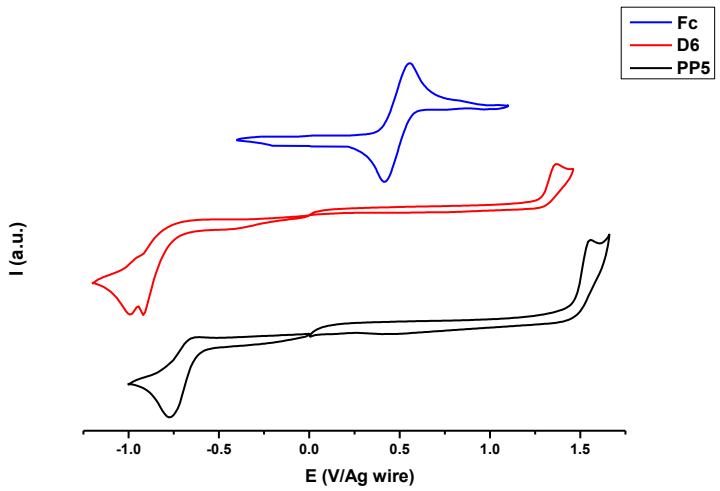

Figure 14. Cyclic voltammograms of **PP5**, **D6** and Ferrocene performed in acetonitrile solutions with tetrabutylammonium perchlorate (0.1 M) as the supporting electrolyte. Scan rate: 100 mV/s.

While getting a deeper insight into the reductions of these compounds, an analogy can be easily made between the electron-withdrawing ability of the acceptor and their reduction potentials. Indeed, the higher the acceptor strength is, the easier the electron acceptor will accept one electron and thus reduce. This capacity is well seen with the different indane derivatives showing easier reduction processes while improving the electron withdrawing ability from **PP5** to **PP17**, as shown in the Figure 15. Parallel to this, elongation of the aromatic core in the indane-based acceptors also improves the accepting properties, as observed for **PP11/D2** and for **PP5/D1**. Addition of one or two dicyanomethylene groups onto the electron acceptors of **PP17**, **PP11** and **D2** favored their reduction at higher cathodic potentials than for their analogues **D1** and **PP5**. These observations are consistent with both theoretical calculations where the electronic density is mostly localized onto the acceptor part i.e. the indane moiety. This is also consistent with the optical properties previously discussed where a red shift of the ICT band is observed, resulting from a decrease of the LUMO energy level. [37,45] In addition, we can highlight the fact that the two most cathodic reduction potentials are found for the two rhodamine derivatives, with almost similar values. This observation proves two phenomena: the fact that the addition of the allyl group has no impact on the accepting ability of the rhodamine group and that rhodanines are extremely weak electron acceptors, in accordance with the observations of their low oxidation potentials. Usually, for push-pull dyes, the HOMO energy level is localized onto the electron donor and the LUMO level is centered onto the accepting moiety. Oppositely, for **D6** and **D7**, an unusual repartition of the two orbitals was

observed by CV and this unexpected behavior was also demonstrated by DFT calculations, the two orbitals extending over the whole molecule. This particularity was also confirmed by the position of their ICT bands greatly differing from that of the other dyes.

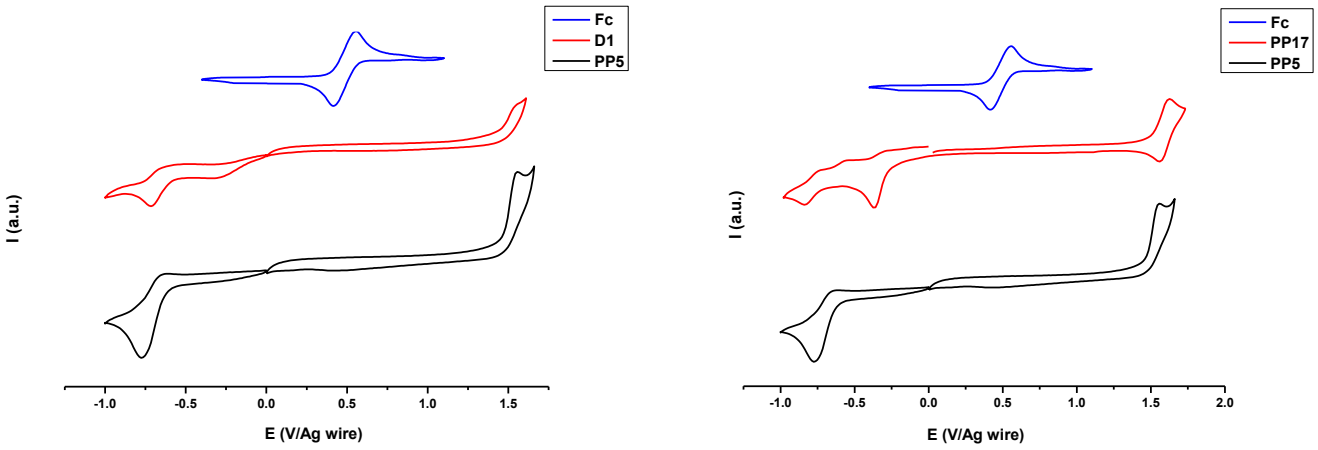

Figure 15. Selected cyclic voltammograms of **PP5**, **PP17**, **D1** and Ferrocene performed in acetonitrile solutions with tetrabutylammonium perchlorate (0.1 M) as the supporting electrolyte. Scan rate: 100 mV/s.

Finally, position of the HOMO and LUMO energy levels could be determined for all dyes. Even though the equations proposed by Pommerehne *et al*. was used, other methods reported in the literature may be mentioned to determine these values such as the equations developed by Cardona *et al*.[78] Indeed, Figure 16 shows a comparison between the frontier orbital energy levels obtained by CV and the energy levels determined by DFT calculations. These data allow us to highlight a few points. Despite a good correlation between CV, UV-visible measurements and DFT calculations, some molecules are better "predicted" than the others. In fact, theoretical values determined for the HOMO energy levels perfectly fit with those determined by cyclic voltammetry with only two exceptions, namely **D8** and **D9** comprising **EA11** and **EA12** as the electron acceptors. To support these variations, and by taking a closer look into the shape of their HOMO orbitals, a higher delocalization of the electronic density can be found for these two dyes compared to the others, which may explain the higher influence of the solvent on the determination of the HOMO position. Indeed, CV measurements were not performed in the same solvent than that used for the theoretical calculations, simply due to the fact that acetonitrile offers a wider electrochemical window than dichloromethane. Finally, considering that the solvent can impact the position of the HOMO energy level, a comparison between the optical and theoretical bandgap in dichloromethane was established. Parallel to this, a comparison between the optical and electrochemical bandgap in

acetonitrile is also provided. As shown in the Figure 17, high differences can be found between the values determined by cyclic voltammetry and absorption spectroscopy. Conversely, a good adequation between the values determined by DFT and absorption spectroscopy can be found. It can be then concluded that ΔE determined by CV is clearly underestimated. This underestimation can be assigned to the difficulty to clearly determine on the cyclic voltammograms the exact positions of the intersection points of the tangents for the oxidation and the reduction potentials. Still differing from the other dyes, a perfect match between the theoretical and optical bandgap could be found for **D6** and **D7** comprising the rhodanine moiety. Indeed, if a difference of about 0.3 eV between the DFT and optical bandgaps can be found for all dyes, this difference is reduced to only 0.1 eV for **D6** and **D7**. An opposite trend was found while comparing the electrochemical and optical bandgaps. In this case, the worse mismatch between the two values can be found for these two compounds. As previously mentioned, **D6** and **D7** drastically differ from the other dyes by their electronic distributions of the HOMO and LUMO energy levels so that a dramatic influence of the solvent on the positions of these two orbitals can be found.

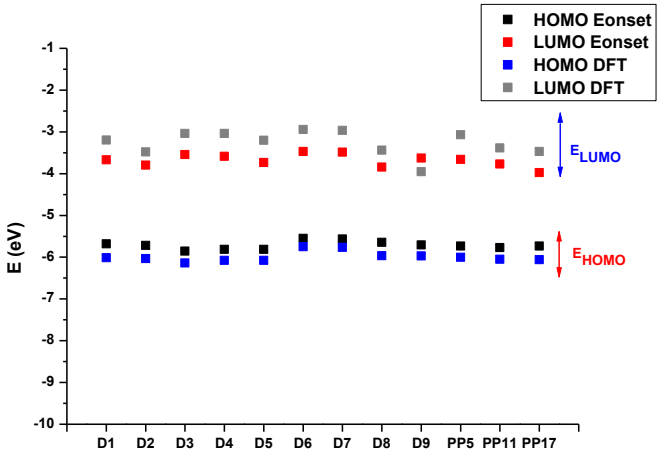

Figure 16. Comparisons between the frontier orbitals' energy levels estimated in acetonitrile by DFT calculations and those obtained by cyclic voltammetry in acetonitrile.

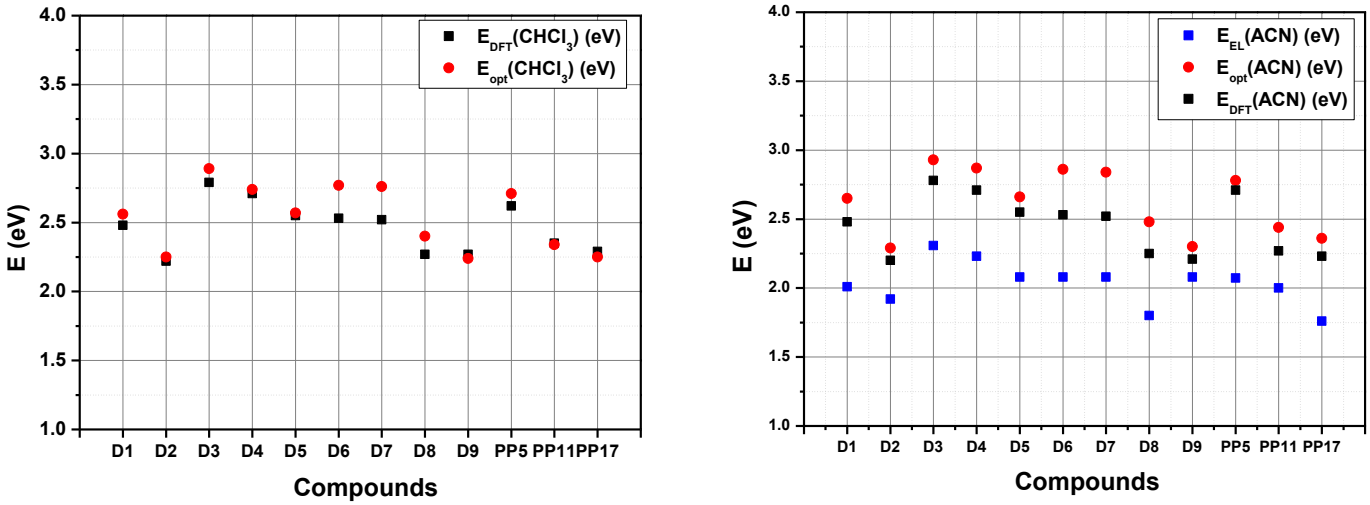

Figure 17. Left: comparisons between the optical determined in chloroform by UV-visible absorption spectroscopy and the theoretical bandgap determined in chloroform by DFT calculations. Right: comparisons of the optical bandgaps determined by UV-visible spectroscopy in acetonitrile, the bandgaps obtained by cyclic voltammetry and theoretical calculations in the same solvent.

Table 6. Summary of the bandgaps determined by UV-visible absorption spectroscopy, cyclic voltammetry and DFT calculations of dyes **A-N**. $E_{ox\ onset}$, correspond to all the oxidation potentials and $E_{red\ onset}$ the reduction potentials. ΔE_{el} corresponds to the difference between the HOMO and the LUMO levels, electrochemically obtained. ΔE_{opt} are calculated from UV bands in different solvents. Finally, ΔE_{th} is the difference between the HOMO and LUMO levels, theoretically obtained. Fc/Fc^{+} was used as internal reference standard.

Compounds	$E_{ox\ onset}$ (V/Fc)	$E_{red\ onset}$ (V/Fc)	E_{HOMO} (eV)	E_{LUMO} (eV)	ΔE_{elACN} (eV)[1]	ΔE_{thACN} (eV)[2]	$\Delta E_{thCHCl3}$ (eV)[3]	$\Delta E_{opt\ ACN}$ (eV)[4]	$\Delta E_{opt\ CHCl3}$ (eV)[5]
D1	0.88	-1.13	-5.68	-3.67	2.01	2.48	2.48	2.65	2.56
D2	0.92	-1.00	-5.72	-3.80	1.92	2.20	2.22	2.29	2.25
D3	1.05	-1.26	-5.85	-3.55	2.31	2.78	2.79	2.93	2.89
D4	1.01	-1.22	-5.81	-3.58	2.23	2.71	2.71	2.87	2.74
D5	1.02	-1.07	-5.82	-3.74	2.08	2.55	2.55	2.66	2.57
D6	0.75	-1.33	-5.55	-3.47	2.08	2.53	2.53	2.86	2.77
D7	0.76	-1.32	-5.56	-3.48	2.08	2.52	2.52	2.84	2.76
D8	0.84	-0.96	-5.64	-3.84	1.80	2.25	2.27	2.48	2.40
D9	0.91	-1.17	-5.71	-3.63	2.08	2.21	2.27	2.30	2.24
PP5	0.93	-1.14	-5.73	-3.66	2.07	2.71	2.62	2.78	2.71
PP11	0.97	-1.03	-5.77	-3.77	2.00	2.27	2.35	2.44	2.34
PP17	0.94	-0.83	-5.74	-3.98	1.76	2.23	2.29	2.36	2.25

[1] All potentials are recorded in 0.1 M $TBAClO_4/CH_3CN$, except for D2 recorded in $TBAClO_4/CH_2Cl_2$. E_{HOMO} (eV) = -4.8 - E_{ox} and E_{LUMO} (eV) = -4.8 - E_{red} [2] Calculated band gaps by DFT in acetonitrile. A dielectric constant of 36.64 was used for the theoretical calculations [3] Calculated band gaps by DFT in chloroform. A dielectric constant

of 4.9 was used for the theoretical calculations [4] Optical bandgaps determined in ACN [5] Optical bandgaps determined in $CHCl_3$

Conclusion

In conclusion, a series of 12 dyes strongly absorbing in the visible range have been synthesized using a weak electron-donor and examined for their photophysical properties. As anticipated, a redshift of the absorption maxima with the acceptor strength was logically observed, enabling the ICT to shift from 447 to 606 nm in chloroform. Examination of their solvatochromism revealed that the different empirical models based on the polarity/polarizability of the solvents could perfectly support the solvatochromism observed experimentally. CV measurements allowed to correlate the trend observed by UV-visible spectroscopy, with a stabilization of the LUMO levels by improving the accepting strength. By electrochemistry, a reduction of these compounds at less cathodic potentials upon improvement of the electron strength was clearly observed. Unusual electrochemical behaviors detected for **D5** and **D6** were supported by DFT calculations evidencing a distribution of both the HOMO and LUMO energy level over the whole molecule. By combining complementary techniques such as UV-visible absorption spectroscopy, DFT calculations and cyclic voltammetry, a better understanding of the photophysical properties could be obtained. Considering their high molar extinction coefficients in solution, some dyes such as **PP5**, **D4** or **D7** are ideal candidates for applications in organic solar cells. However, their absorptions in thin films, especially when mixed with an electron acceptor such as [6,6]-phenyl-C_{61}-butyric acid methyl ester ($PC_{61}BM$), the nanostructuration in bulk heterojunctions have still to be examined.[79-81] Parallel to this, panchromatic dyes are also actively researched for photopolymerization applications. In this field, **PP6**, **D9** and **D10** by their broad absorption spectra extending over the visible range are perfect candidates and polymerization tests for the free radical polymerization of acrylates or the cationic polymerization of epoxides under low light intensity and even for sunlight-induced polymerization will be reported in forthcoming works. However, the absorption properties of dyes are not the only parameters governing the polymerization efficiencies.[19,20] Notably, the rate constants of interactions with the different additives introduced in the three-component photoinitiating systems, the possibility of back electron transfer between the excited photosensitizers and the additives, or the solubility of dyes in monomers cannot be anticipated at this stage so that comparisons with benchmark systems have to be precluded.

Acknowledgments

The authors thank Aix Marseille University and The Centre National de la Recherche Scientifique (CNRS) for financial supports. The Agence Nationale de la Recherche (ANR agency) is acknowledged for its financial support through the PhD grants of Corentin Pigot (ANR-17-CE08-0010 DUALITY project) and Guillaume Noirbent (ANR-17-CE08-0054 VISICAT project).

References

[1] Chou, P.-T.; Chi, Y. Phosphorescent dyes for organic light-emitting diodes, Chem. Eur. J. 2007;13:380-395.

[2] Redon, S.; Eucat, G.; Ipuy, M.; Jeanneau, E.; Gautier-Luneau, I.; Ibanez, A.; Andraud, C.; Bretonnière, Y.; Tuning the solid-state emission of small push-pull dipolar dyes to the far-red through variation of the electron-acceptor group, Dyes Pigm. 2018;156:116-132.

[3] Hancock, J.M.; Gifford, A.P.; Zhu, Y.; Lou, Y. Jenekhe, S.A. n-Type conjugated oligoquinoline and oligoquinoxaline with triphenylamine endgroups: efficient ambipolar light emitters for device applications, Chem. Mater. 2006;18:4924-4932.

[4] Farré, Y.; Raissi, M.; Fihey, A.; Pellegrin, Y.; Blart, E.; Jacquemin, D.; Odobel, F. Synthesis and properties of new benzothiadiazole-based push-pulldyes for p-type dye sensitized solar cells, Dyes Pigm. 2018;148:154-166.

[5] Parsa, Z.; Shahab Naghavi, S.; Safari, N. Designing push−pull porphyrins for efficient dye-sensitized solar cells, J. Phys. Chem. A 2018;122:5870-5877.

[6] Yella, A.; Mai, C.-L.; Zakeeruddin, S.M.; Chang, S.-N.; Hsieh, C.-H.; Yeh, C.-Y.; Graetzel, M. Molecular engineering of push–pull porphyrin dyes for highly efficient dye-sensitized solar cells: the role of benzene spacers, Angew. Chem. Int. Ed. 2014;53:2973-2977.

[7] Huo, F.; Zhang, H.; Chen, Z.; Qiu, L.; Liu, J.; Bo, S.; Kityk, I.V. Novel nonlinear optical push–pull fluorene dyes chromophore as promising materials for telecommunications, J. Mater. Sci. Mater. Electron. 2019;30:12180-12185.

[8] Raimundo, J.M.; Blanchard, P.; Gallego-Planas, N.; Mercier, N.; Ledoux-Rak, I.; Hierle, R.; Roncali, J. Design and synthesis of push-pull chromophores for second-order

nonlinear optics derived from rigidified thiophene-based-conjugating spacers, J. Org. Chem. 2002;67:205-218.

[9] Mohammed, N.; Wiles, A.A.; Belsley, M.; Fernandes, S.S.M.; Cariello, M.; Rotello, V.M.; Raposo, M.M.M.; Cooke, G. Synthesis and characterisation of push-pull flavin dyes with efficient second harmonic generation (SHG) properties, RSC Adv. 2017;7:24462-24469.

[10] Thooft, A.M.; Cassaidy, K.; Van Veller, B. A small push−pull fluorophore for turn-on fluorescence, J. Org. Chem. 2017;82:8842-8847.

[11] Karpenko, I.A.; Niko, Y.; Yakubovskyi, V.P.; Gerasov, A.O.; Bonnet, D.; Kovtun, Y.P.; Klymchenko, A.S. Push-pull dioxaborine as fluorescent molecular rotor: far-red fluorogenic probe for ligand–receptor interactions, J. Mater. Chem. C 2016;4:3002-3009.

[12] Xiao, P.; Dumur, F.; Bui, T.-T.; Sallenave, X.; Goubard, F.; Graff, B.; Morlet-Savary, F.; Fouassier, J.-P.; Gigmes, D.; Lalevée, J. Panchromatic photopolymerizable cationic films using indoline and squaraine dyes based photoinitiating systems, ACS MacroLetters 2013;2:736-740.

[13] Tehfe, M.-A.; Dumur, F.; Vilà, N.; Graff, B.; Mayer, C.R.; Fouassier, J.-P.; Gigmes, D.; Lalevée, J. A multicolor photoinitiator for cationic polymerization and interpenetrated polymer network synthesis: 2,7-di-*tert*-butyldimethyl-dihydropyrene, Macromol. Rapid Commun. 2013;34:1104-1109.

[14] Xiao, P.; Dumur, F.; Thirion, D.; Fagour, S.; Vacher, A.; Sallenave, X.; Graff, B.; Fouassier, J.-P.; Gigmes, D.; Lalevée, J. Multicolor photoinitiators for radical and cationic polymerization: mono vs. poly functional thiophene derivatives, Macromolecules 2013;46:6786-6793.

[15] Tehfe, M.-A.; Dumur, F.; Graff, B.; Morlet-Savary, F.; Gigmes, D.; Fouassier, J.-P.; Lalevée, J. Push-pull (thio)barbituric acid derivatives in dye photosensitized radical and cationic polymerization reactions under 457/473 nm Laser beams or blue LEDs, Polym. Chem. 2013;4:3866-3875.

[16] Xiao, P.; Dumur, F.; Graff, B.; Vidal, L.; Gigmes, D.; Fouassier, J.-P.; Lalevée, J. Structural effects in the indanedione skeleton for the design of low intensity 300-500 nm light sensitive initiators, Macromolecules 2014;47:26-34.

[17] Xiao, P.; Dumur, F.; Tehfe, M.-A.; Gigmes, D.; Fouassier, J.-P.; Lalevée, J. Red-light-induced cationic photopolymerization: perylene derivatives as efficient photoinitiators, Macromol. Rapid. Commun. 2013;34:1452-1458 .

[18] Al Mousawi, A.; Poriel, C.; Dumur, F.; Toufaily, J.; Hamieh, T.; Fouassier, J.-P.; Lalevée, J. Zinc tetraphenyl-porphyrin as high performance visible-light photoinitiator of cationic photosensitive resins for LED projector 3D printing applications, Macromolecules 2017;50:746−753.

[19] Pigot, C.; Noirbent, G.; Brunel, D.; Dumur, F. Recent advances on push-pull organic dyes as visible light photoinitiators of polymerization, Eur. Polym. J. 2020;133:109797.

[20] Dumur, F. Recent advances on visible light photoinitiators of polymerization based on indane-1,3-dione and related derivatives, Eur. Polym. J. 2021;143:110178.

[21] Lalevée, J.; Fouassier, J.-P. Recent advances in sunlight induced polymerization: role of new photoinitiating systems based on the silyl radical chemistry, Polym. Chem., 2011;2:1107-1113.

[22] Tehfe, M.-A.; Lalevée, J.; Gigmes, D.; Fouassier, J.-P. Green Chemistry: Sunlight-Induced Cationic Polymerization of Renewable Epoxy Monomers Under Air, Macromolecules 2010;43:1364-1370.

[23] Sun, K.; Liu, S.; Chen, H.; Morlet-Savary, F.; Graff, B.; Pigot, C.; Nechab, M.; Xiao, P.; Dumur, F.; Lalevée, J. N-ethylcarbazole-1-allylidene-based push-pull dyes as efficient light harvesting photoinitiators for sunlight induced polymerization, Eur. Polym. J. 2021;147:110331.

[24] Tehfe, M.-A.; Louradour, F.; Lalevée, J.; Fouassier, J.-P. Photopolymerization Reactions: On the Way to a Green and Sustainable Chemistry, Appl. Sci. 2013;3:490-514.

[25] Lalevée, J.; Mokbel, H.; Fouassier, J.-P. Recent Developments of Versatile Photoinitiating Systems for Cationic Ring Opening Polymerization Operating at Any Wavelengths and under Low Light Intensity Sources, Molecules 2015;20:7201-7221.

[26] Dietlin, J.; Schweizer, S.; Xiao, P.; Zhang, J.; Morlet-Savary, F.; Graff, B.; Fouassier, J.-P.; Lalevée, J. Photopolymerization upon LEDs: new photoinitiating systems and strategies, Polym. Chem. 2015;6:3895-3912.

[27] Ravelli, D.; Fagnoni, M. Dyes as visible light photoredox organocatalysts, ChemCatChem 2012;4:169-171.

[28] Le, T.; Courant, T.; Merad, J.; Allain, C.; Audebert, P.; Masson, G. s-Tetrazine dyes: A facile generation of photoredox organocatalysts for routine oxidations, J. Org. Chem. 2019;84:16139-16146.

[29] Fidaly, K.; Ceballos, C.; Falguières, A.; Sylla-Iyarreta Veitia, M.; Guy, A.; Ferroud, C. Visible light photoredox organocatalysis: a fully transition metal-free direct asymmetricα-alkylation of aldehydes, GreenChem. 2012;14:1293-1297.

[30] da Gama Oliveira, V.; Filomena do Carmo Cardoso, M.; da Silva Magalhães Forezi, L. Organocatalysis: A brief overview on its evolution and applications, Catalysts 2018;8:605.

[31] Bureš, F. Fundamental aspects of property tuning in push–pull molecules, RSC Adv. 2014;4:58826-58851.

[32] Kulhanek, J.; Bures, F.; Pytela, O.; Mikysek, T.; Ludvıkc, J.; Ruzicka, A. Push-pull molecules with a systematically extended p-conjugated system featuring 4,5-dicyanoimidazole, Dyes Pigm. 2010;85:57-65.

[33] Kuhn, H. Oscillator strength of absorption band in dye molecules, J. Chem. Phys. 1958;29:958.

[34] Feng, J.; Jiao, Y.; Ma, W.; Nazeeruddin, M.K.; Grätzel, M.; Meng, S. First principles design of dye molecules with ullazine donor for dye sensitized solar cells, J. Phys. Chem. C 2013;117:3772-3778.

[35] Thomas, R.; Thomas, A.; Pullanchery, S.; Joseph, L.; Mambully Somasundaran, S.; Srinivasamurthy Swathi, R.; Gray, S.K.; George Thomas, K. Plexcitons: The role of oscillator strengths and spectral widths in determining strong coupling ACS Nano 2018;12:402-415.

[36] Francos, J.; Borge, J.; Diez, J.; Garcia-Garrido, S.E.; Cadierno, V. Easy entry to donor/acceptor butadiene dyes through a MW-assisted InCl3-catalyzed coupling of propargylic alcohols with indan-1,3-dione in water Catal. Commun. 2015;63:10-14.

[37] Francos, J.; Garcıa-Garrido, S.E.; Borge, J.; Suarez, F.J.; Cadierno, V. Butadiene dyes based on 3-(dicyano-methylidene)indan-1-one and 1,3-bis(dicyanomethylidene)indane: synthesis, characterization and solvatochromic behavior, RSC Adv. 2016;6:6858-6867.

[38] Barnsley, J.E.; Pelet, W.; McAdam, J.; Wagner, K.; Hayes, P.; Officer, D.L.; Wagner, P.; Gordon, K.C. When "donor−acceptor" dyes delocalize: A spectroscopic and computational study of D−A dyes using "Michler's Base", J. Phys. Chem. A 2019;123:5957-5968.

[39] Cadierno, V. (E)-1,1,1-Trifluoro-6,6-bis(4-methoxyphenyl)hexa-3,5-dien-2-one, Molbank 2020;2020:M1120.

[40] Dumur, F.; Mayer, C.R.; Dumas, E.; Miomandre, F.; Frigoli, M.; Sécheresse, F. New chelating stilbazonium like dyes from Michler's ketone, Org. Lett. 2008;10:321-324.

[41] Tehfe, M.-A.; Dumur, F.; Graff, B.; Morlet-Savary, F.; Gigmes, D.; Fouassier, J.-P.; Lalevée, J. New push-pull dyes derived from Michler's ketone for polymerization reactions upon visible lights, Macromolecules 2013;46:3761-3770.

[42] Mokbel, H.; Dumur, F.; Graff, B.; Gigmes, D.; Mayer, C.R.; Toufaily, J.; Hamieh, T.; Fouassier, J.-P.; Lalevée, J. Michler's ketone as an interesting scaffold for the design of high-performance dyes in photoinitiating systems upon visible lights, Macromol. Chem. Phys. 2014;215:783-790.

[43] Noirbent, G.; Dumur, F. Recent advances on nitrofluorene derivatives: Versatile electron acceptors to create dyes absorbing from the visible to the near and far infrared region, Materials 2018;11:2425.

[44] Knoevenagel, E. Ueber eine Darstellungsweise des Benzylidenacetessigesters, Ber. Dtsch. Chem. Ges. 1896;29 :172-174.

[45] Pigot, C.; Noirbent, G.; Peralta, S.; Duval, S.; Bui, T.-T.; Aubert, P.-H.; Nechab, M.; Gigmes, D.; Dumur, F. New push-pull dyes based on 2-(3-oxo-2,3-dihydro-1H-cyclopenta[b]naphthalen-1-ylidene)malononitrile: An amine-directed synthesis, Dyes Pigm. 2020;175:108182.

[46] Pigot, C.; Noirbent, G.; Peralta, S.; Duval, S.; Nechab, M.; Gigmes, D.; Dumur, F. Unprecedented nucleophilic attack of piperidine on the electron acceptor during the

synthesis of push-pull dyes by a knoevenagel reaction, Helv. Chim. Acta 2019;102:e1900229.

[47] Landmesser, T.; Linden, A.; Hansen, H.-J.; A novel route to 1-substituted 3-(dialkylamino)-9-oxo-9H-indeno[2,1-c]-pyridine-4-carbonitriles. Helv. Chim. Acta 2008;91:265-284.

[48] Helmy, S.; Oh, S.; Leibfarth, F.A.; Hawker, C.J.; Read de Alaniz, J. Design and synthesis of donor-acceptor Stenhouse adducts: a visible light photoswitch derived from furfural. J. Org. Chem. 2014;79:11316-11329.

[49] Gao, M.; Su, H.; Lin, Y.; Ling, X.; Li, S.; Qin, A.; Zhong Tang, B. Photoactivatable aggregation-induced emission probes for lipid droplets-specific live cell imaging, Chem. Sci. 2017;8:1763-1768.

[50] Cui, Y.; Ren, H.; Yu, J.; Wang, Z.; Qian, G; An indanone-based alkoxysilane dye with second order nonlinear optical properties, Dyes Pigm. 2009;81:53-57.

[51] Yang, X.; Fox, T.; Berke, H. Synthetic and mechanistic studies of metal-free transfer hydrogenations applying polarized olefins as hydrogen acceptors and amine borane adducts as hydrogen donors, Org. Biomol. Chem. 2012;10:852-860.

[52] Pigot, C.; Noirbent, G.; Bui, T.-T.; Peralta, S.; Duval, S.; Gigmes, D.; Nechab, M.; Dumur, F. Synthesis, optical and electro-chemical properties of a series of push-pull dyes based on the 4-(9-ethyl-9H-carbazol-3-yl)-4-phenylbuta-1,3-dienyl donor, New J. Chem. (2021) 10.1039/D1NJ00275A

[53] Pigot, C.; Noirbent, G.; Peralta, S.; Duval, S.; Nechab, M.; Gigmes, D.; Dumur, F. Unprecedented nucleophilic attack of piperidine on the electron acceptor during the synthesis of push-pull dyes by a knoevenagel reaction, Helv. Chim. Acta 2019;102:e1900229.

[54] Cao, C.; Zhou, X.; Xue, M.; Han, C.; Feng, W.; Li, F. Dual near-infrared-emissive luminescent nanoprobes for ratiometric luminescent monitoring of ClO− in living organisms, ACS Appl. Mater. Interf. 2019;11:15298-15305.

[55] Perepichka, D.F.; Perepichka, I.F.; Ivasenko, O.; Moore, A.J.; Bryce, M.R.; Kuzmina, L.G.; Batsanov, A.S.; Sokolov, N.I. Combining high electron affinity and

intramolecular charge transfer in 1,3-dithiole–nitrofluorene push–pull diads, Chem. Eur. J. 2008;14:2757-2770.

[56] Pavelyev, V.G.; Parashchuk, O.D.; Krompiec, M.; Orekhova, T.V.; Perepichka, I.F.; van Loosdrecht, P.H.M.; Paraschuk, D.Y.; Pshenichnikov, M.S. Charge transfer dynamics in donor−acceptor complexes between a conjugated polymer and fluorene acceptors, J. Phys. Chem. C 2014;118:30291-30301.

[57] Frisch, M.J.; Trucks, G.W.; Schlegel, H.B.; Scuseria, G.E.; Robb, M.A.; Cheeseman, J.R.; Montgomery, Jr., J.A.; Vreven, T.; Kudin, K.N.; Burant, J.C.; Millam, J.M.; Iyengar, S.S.; Tomasi, J.; Barone, V.; Mennucci, B.; Cossi, M; Scalmani, G.; Rega, N.; Petersson, G.A.; Nakatsuji, H.; Hada, M.; Ehara, M.; Toyota, K.; Fukuda, R.; Hasegawa, J.; Ishida, M.; Nakajima, T.; Honda, Y.; Kitao, O.; Nakai, H.; Klene, M.; Li, X.; Knox, J.E.; Hratchian, H.P.; Cross, J.B.; Bakken, V.; Adamo, C.; Jaramillo, J.; Gomperts, R.; Stratmann, R.E.; Yazyev, O.; Austin, A.J.; Cammi, R.; Pomelli, C.; Ochterski, J.W.; Ayala, P.Y.; Morokuma, K.; Voth, G.A.; Salvador, P.; Dannenberg, J.J.; Zakrzewski, V.G.; Dapprich, S.; Daniels, A. D.; Strain, M.C.; Farkas, O.; Malick, D.K.; Rabuck, A.D.; Raghavachari, K.; Foresman, J.B.; Ortiz, J.V.; Cui, Q.; Baboul, A.G.; Clifford, S.; Cioslowski, J.; Stefanov, B.B.; Liu, G.; Liashenko, A.; Piskorz, P.; Komaromi, I.; Martin, R.L.; Fox, D.J.; Keith, T.; Al-Laham, M.A.; Peng, C.Y.; Nanayakkara, A.; Challacombe, M.; Gill, P.M.W.; Johnson, B.; Chen, W.; Wong, M.W.; Gonzalez, C.; Pople, J.A. Gaussian, Inc., Wallingford CT, 2009

[58] C. Lee, W. Yang, R.G. Parr, Development of the Colle-Salvetti correlation-energy formula into a functional of the electron density. Phys. Rev. B. Condens. Matter. 1988;37:785-789

[59] A.D. Becke, A new mixing of Hartree–Fock and local density-functional theories J. Chem. Phys. 1993;98:1372-1377.

[60] W.J. Hehre, R. Ditchfield, J.A. Pople, Self-consistent molecular orbital methods. XII. Further extensions of Gaussian-type basis sets for use in molecular orbital studies of organic molecules. J. Chem. Phys. 1972;56:2257-2261.

[61] J. Tomasi, B. Mennucci, E. Cances, The IEF version of the PCM solvation method: an overview of a new method addressed to study molecular solutes at the QM ab initio level. J. Mol. Struct. THEOCHEM 1999;464:211-226.

[62] G. Scalmani, M.J. Frisch, Continuous surface charge polarizable continuum models of solvation. I. General formalism. J. Chem. Phys. 2010;132:114110.

[63] N.M. O'Boyle, A.L. Tenderholt, K.M. Langner, cclib: A library for package-independent computational chemistry algorithms. J. Comp. Chem. 2008;29:839-845. https://doi.org/10.1002/jcc.20823

[64] Kurdyukova, I.V.; Ishchenko, A.A.; Derevyanko, N. A.; Mysyk, D.D. synthesis and spectral properties of merocyanine dyes derived from tetra-nitrofluorene and heterocycles of various electron-donating ability, Chem. Heterocycl. Comp. 2013;49, 281–293.

[65] Kamlet, M.J.; Abboud, J.-L.M.; Abraham, M.H.; Taft, R.W. Linear solvation energy relationships. 23. A comprehensive collection of the solvatochromic parameters, .pi.*, .alpha., and .beta., and some methods for simplifying the generalized solvatochromic equation, J. Org. Chem. 1983;48:2877-2887.

[66] Reichardt, C. Solvatochromic Dyes as Solvent Polarity Indicators. Chem. Rev. 1994;94:2319-2358.

[67] Lippert, E.Z. Dipolmoment und Elektronenstruktur von angeregten Molekülen. Naturforsch. 1955;10a:541-545 http://zfn.mpdl.mpg.de/data/Reihe_A/10/ZNA-1955-10a-0541.pdf

[68] Catalan, J. On the ET (30), π*, Py, S‘, and SPP empirical scales as descriptors of nonspecific solvent effects J. Org. Chem. 1997;62 :8231-8234

[69] Catalan, J.; Lopez, V.; Perez, P.; Matin-Villamil, R.; Rodriguez, J. G. Progress towards a generalized solvent polarity scale: The solvatochromism of 2-(dimethylamino)-7-nitrofluorene and its homomorph 2-fluoro-7-nitrofluorene, Liebigs Ann. 1995 ;2:241-252.

[70] Kawski, A. Zur lösungsmittelabhängigkeit der wellenzahl von elektronenbanden lumineszierender moleküle und über die bestimmung der elektrischen dipolmomente im anregungszustand. Acta Phys. Polon. 1966;29:507-518.

[71] Mcrae, e.g. theory of solvent effects on molecular electronic spectra. frequency shifts, J. Phys. Chem. 1957;61:562-572.

[72] Suppan, P. Solvent effects on the energy of electronic transitions: experimental observations and applications to structural problems of excited molecules, J. Chem. Soc. A 1968:3125-3133.

[73] Bakshiev, N.G. Universal intermolecular interactions and their effect on the position of the electronic spectra of molecules in two component solutions, Opt. Spektrosk. 1964;16:821-832.

[74] Catalan, J. Toward a generalized treatment of the solvent effect based on four empirical scales: dipolarity (SdP, a new scale), polarizability (SP), acidity (SA), and basicity (SB) of the medium, J. Phys. Chem. B 2009;113:5951-5960.

[75] del Valle, J.C.; García Blanco, F.; Catalán, J. Empirical parameters for solvent acidity, basicity, dipolarity, and polarizability of the ionic liquids [BMIM][BF4] and [BMIM][PF_6], J. Phys. Chem. B 2015;119:4683-4692.

[76] Palomar, J.; Torrecilla, J.S.; Lemus, J.; Ferro, V.R.; Rodriguez, F. Prediction of non-ideal behavior of polarity/ polarizability scales of solvent mixtures by integration of a novel COSMO-RS molecular descriptor and neural networks, Phys. Chem. Chem. Phys. 2008;10:5967-5975.

[77] Pommerehne, J.; Vestweber, H.; Guss, W.; Mahrt, R. F.; Bässler, H.; Porsch, M.; Daub, J. Efficient Two Layer Leds on a Polymer Blend Basis. Advanced Materials 1995, 7 (6), 551–554.

[78] Cardona, C. M.; Li, W.; Kaifer, A. E.; Stockdale, D.; Bazan, G. C. Electrochemical Considerations for Determining Absolute Frontier Orbital Energy Levels of Conjugated Polymers for Solar Cell Applications. Adv. Mater. 2011, 23 (20), 2367–2371.

[79] Alam, S.; Shaheer Akhtar, M.; Abdullah, A.; Kim, E.-B.; Shin, H.-S.; Ameen, S. Planar D-π-A configured dimethoxy vinylbenzene based small organic molecule for solution-processed bulk heterojunction organic solar cells, Appl. Sci. 2020, 10, 5743.

[80] Liu, Y.; Sun, Y.; Li, M.; Feng, H.; Ni, W.; Zhang, H.; Wan, Y.; Chen, Y. Efficient carbazole-based small-molecule organic solar cells with an improved fill factor, RSC Adv. 2018, 8, 4867–4871.

[81] Roquet, S.; Cravino, A.; Leriche, P.; Alévêque, O.; Frère, P.; Roncali, J. Triphenylamine-Thienylenevinylene Hybrid Systems with Internal Charge Transfer as

Donor Materials for Heterojunction Solar Cells, J. Am. Chem. Soc. 2006, 128, 3459-3466.